The effect of samara seed wing flexibility on its aerodynamic performance

Final Report

The University of Manchester

Department of Mechanical, Aerospace and Civil Engineering 2021-22

Project Supervisor: Mostafa Nabawy

Bartlomiej Hasko, 10540264

Contents

Table of Figures

FIGURE 18 Descent velocity with relation to the samara seed mass for e = 1*10^9 .36

Nomenclature

A	Rotor disc area, A
AR	Aspect ratio
c	Blade mean chord
c_r	Root chord length
δc	Local chord length
C_d	3D drag coefficient
C_L	3D lift coefficient
$C_{L,v}$	Vortex lift coefficient
$C_{L,p}$	Potential lift coefficient
$C_{l\alpha,2D}$	2D lift curve slope constant
$C_{l\alpha,3D}$	3D lift curve slope
δD	Incremental drag acting on a blade element
e	Euler's number
E	Edge correction factor
F_c	Centrifugal force
$F_{cr}(i)$	Incremental centrifugal force acting on a blade element due to its mass
F_{cs}	Centrifugal force due to the seed's mass
F_{cT}	Sum of in-plane components of incremental thrust force
$F_g(i)$	Component of force of gravity acting on a blade element normal to the wing
g	Gravitational constant
I	Second moment of area for a rectangular shape
$I(i)$	Second moment of area of a blade element
k	Induced power factor
k_{flap}	Flapping induced factor
k_{ind}	Non-uniform downwash induced factor
k_{tip}	Tip loss induced factor
K_i	Induced lift coefficient constant
K_p	Potential lift coefficient constant
δL	Incremental lift acting on a blade element
$mass_p(i)$	Mass of each blade element

M	Mass of the samara seed
Q	Sum of the incremental torques acting on the wing
δQ	Incremental torque
r	Radial distance from the centre of rotation
$r(i)$	Distance of a blade element radial position to the centre of rotation
δr	Distance of a blade element radial position to the centre of rotation
T	Thrust normal to the datum plate
δT	Incremental thrust normal to the wing
T_m	Thrust predicted by the momentum analysis
$thickness_i\ (j)$	Thickness at a sampling point where i is the spanwise point number and j is the chordwise point number
$thickness(i)$	Total thickness of all local chordwise points at a certain radial position
U	Incoming flow velocity
U_p	Up-flow component of the incoming flow velocity normal to the plane
U_T	In-plane component of the incoming flow velocity tangential to the plane
v_i	Induced velocity
$v_i(\hat{r})$	Downwash velocity distribution
V_d	Vertical descent velocity of the samara seed

Greek Symbols

α	Angle of attack
β	Coning angle relative to the datum plane
$\dot{\beta}$	Blade flapping angle
$\beta(i)$	Local blade element coning angle
$\beta_\delta(i)$	Local blade element coning angle change due to deflection
ω	Angular velocity
Λ	Sweep angle
ρ	Air density
ϕ	Local inflow angle
η_{tip}	Tip loss coefficient

θ	Blade pitch angle
$\delta(i)$	Deflection of a blade element

Abstract

There has been an increasing interest in the implementation of samara seed flight characteristics into aerial vehicles. Extensive research has already been conducted on the natural samara seeds, however, its implementation in drones or helicopters is still lacking. In this paper, a study about the influence of the structural properties of samara seed on its flight performance has been undertaken. The insights achieved in this study aim to help in the future design of samara seed-like wings. A careful literature review has been conducted of the available research and the main finding have been described. Based on the acquired knowledge, an analytical model has been developed and coded in Matlab. The code allowed for the extraction of key graphs that depicted the influence of the samara seed structure on its wing flight performance. It has been found that there is a correlation between the samara seed material's Young's modulus and its descent velocity. However, further work is still required to assess the influence of other material properties.

1 Introduction

1.1 Background

Samara seed is a seed that has developed a wing-like structure to enhance its germination distance. Evolution has shaped these wings to achieve stable autorotation to decrease its descent velocity. Therefore, these wings can achieve greater dispersion and populate larger areas to ensure an optimal distance between each other. Such seeds are commonly met in our daily life as some examples contain maple or elm. The focus of research, that has been done into these seeds, is their incredible flight properties. Additionally, some of the research that has been done on insect wings can also be applied to samara seed wings, since there are many similarities between them. Understanding samara seed flight is key to taking advantage of the properties that nature has developed over thousands of years. Some distinct features of these wings are their ability to autorotate, operate at high angles of attack, and structurally "fibrous" wings. The autorotation that is autonomously achieved in the first seconds of their descent and their ability to sustain such flight conditions is a careful balance between inertia, kinematics, and aerodynamics. The aerodynamics of the wing focus its attention on the way these wings generate lift, as models that are commonly used in conventional aircraft do not accurately describe the way these wings operate. These models are not accurate mainly due to the leading-edge vortex (LEV) that this wing develops. Such vortices also occur on delta wings and helicopter blades. The primary focus has been to explain its relevance in samara seed flight. There are some models that describe how LEVs contribute to the lift generated by the wing. They can be divided into two different theories: additional lift and absence of stall (Nabawy MRA, Crowther WJ., 2017). The research done in this area has been quite extensive and samara seeds can also be accurately simulated in CFD software, which indicates that there is little research to be done in this area.

1.2 Motivation

The in-depth understanding of samara seed flight is not only driven by human curiosity, but also by the ability to apply what we learn to our advantage. The extraordinary abilities of samara seeds can help us develop new technologies that will ensure better safety and performance of aerial vehicles. An example of one application is autorotation. This could ensure the safety of passengers on vehicles that create lift through rotating blades. Once a catastrophic failure occurs, these aircraft plummet to the ground and all passengers usually die. However, with implemented autorotation,

these vehicles would become much safer, as the descent would become much slower, and some passengers could survive. Another example of an application is drones.

Figure 1 Samara seed drone (S. K. H. Win, L. S. T. Win, D. Sufiyan, G. S. Soh and S. Foong, 2019)

They could mimic the samara seed flight altogether and could prove to be beneficial when compared to conventional drones in some areas. Therefore, a better understanding of samara seed flight will help us achieve these results. This paper aims to improve the understanding of samara seed flight that could benefit the future design of new technologies. This will be done through a study of the samara seed wing structure. This distinct feature of samara seeds has not been given equal attention as its aerodynamics or autorotation. The structure's shape plays a vital role in the way the aerodynamic forces act and influence the kinematics that drive the autorotation. There have been studies that focused on the samara seed shape and how it influences the performance of the samara seed flight. One such study has been made by Evan R Ulrich et al. (2010) where they have studied how different samara seed structural properties influence its flight path and the descent velocity. However, there are still unknowns that must be addressed. One such unknown is how a varying material stiffness would influence the samara seed flight. Such a study is necessary to assess what material properties are best in terms of performance for the design of such an artificial samara seed wing. This paper will focus on this aim and try to provide some insight into how the material properties of samara seed wing will influence samara seed performance.

2 Literature Review

2.1 Aerodynamic models

A few theories that describe samara seed aerodynamics have been developed and, according to Nabawy MRA and Crowther WJ 2017, they can be divided into two different types of models. The additional lift model is based on the theory that the leading-edge vortex circulation increases the maximum possible lift in comparison to the lift that would be generated in its absence. The second, absence of stall model, states that LEV replaces the potential flow solution and allows for the flow to be attached at high angles of attack (Nabawy MRA, Crowther WJ, 2017). One example of each model will be described in this paper. A model developed by Rezgui D. et al. (2020) can be classified as the additional lift theory. It was based on the Polhamus' model that describes the formation of LEVs on finite wings (Rezgui D. et al. 2020). Polhamus' model states that the LEVs force is a suction force that acts normal to the wing when the flow remains attached and satisfies the Kutta condition at the leading edge (Polhamus, 1966). In this model, the lift is created by two different components: the potential flow component and the vortex lift component. Rezgui D et al. (2020) apply this theory to the samara seed wing and then use the blade element method (BEM) to calculate the 3D lift coefficient for a specified wing. In their' paper, the potential lift coefficient is equal to

$$C_{L,p} = K_p \sin(\alpha)\cos^2(\alpha) \approx \frac{\partial C_{L,p}}{\partial \alpha}\alpha \tag{1}$$

where $C_{L,p}$ can be derived by an application of any appropriate lifting-surface theory for small angles of attack. The vortex lift component is specified to be

$$C_{L,v} = (K_p - {K_p}^2 K_i)\frac{\cos(\alpha)}{\cos(\Lambda)} sin^2(\alpha) \tag{2}$$

where Λ is the sweep angle assumed to be zero for samara seed application. Since the total 2D lift coefficient is composed of the potential and the vortex lift coefficient, its equation is as follows:

$$C_L(\alpha) = K_p \sin(\alpha)\cos^2(\alpha) + (K_p - {K_p}^2 K_i)\frac{\cos(\alpha)}{\cos(\Lambda)} sin^2(\alpha) \tag{3}$$

This equation was later applied along with a kinematic model and BEM theory in MATLAB. Further explanations of these will be found in later sections as similar solutions have been implemented in this paper's study. The other relevant aerodynamic

model that has been developed by Nabawy MRA and Crowther WJ, 2017 is an example of an absence of stall model. They have developed a normal force model that is a modified potential force model. Their theory includes a correction for the coefficient of lift that drives its value to 0 at 90° angle of attack. The modified equation is equal to

$$C_l = C_{L\alpha,2D} \sin\alpha \cos\alpha. \quad (4)$$

Their study follows with a comparison of the normal force model to the suction force model and potential flow model. The suction force model is based on the Polhamus approach to the LEV in delta wings, therefore it is similar to the model that has been developed by Rezgui D et al. (2020). These theories are then applied to the wings of different animals and insects. It was found that the normal force model represents the experimental and computational findings most accurately. Samara seed wings are very similar to the wings that have been used in that study and it is possible to apply the same models to them. That is why the aerodynamic model that has been developed by Nabawy MRA and Crowther WJ in 2014A, 2014B, and 2017 papers will be applied as the aerodynamic model in this paper.

2.2 Kinematic model

A kinematic model describes how aerodynamic forces developed by a samara seed wing act on its structure. It allows to understand how a samara seed forms a stable autorotational flight. One of such models has been developed by Rezgui D. et al. (2020)

to create a MATLAB code that can output the rotational, downwash, and descent velocity of a samara seed. A visual description of this model is presented below.

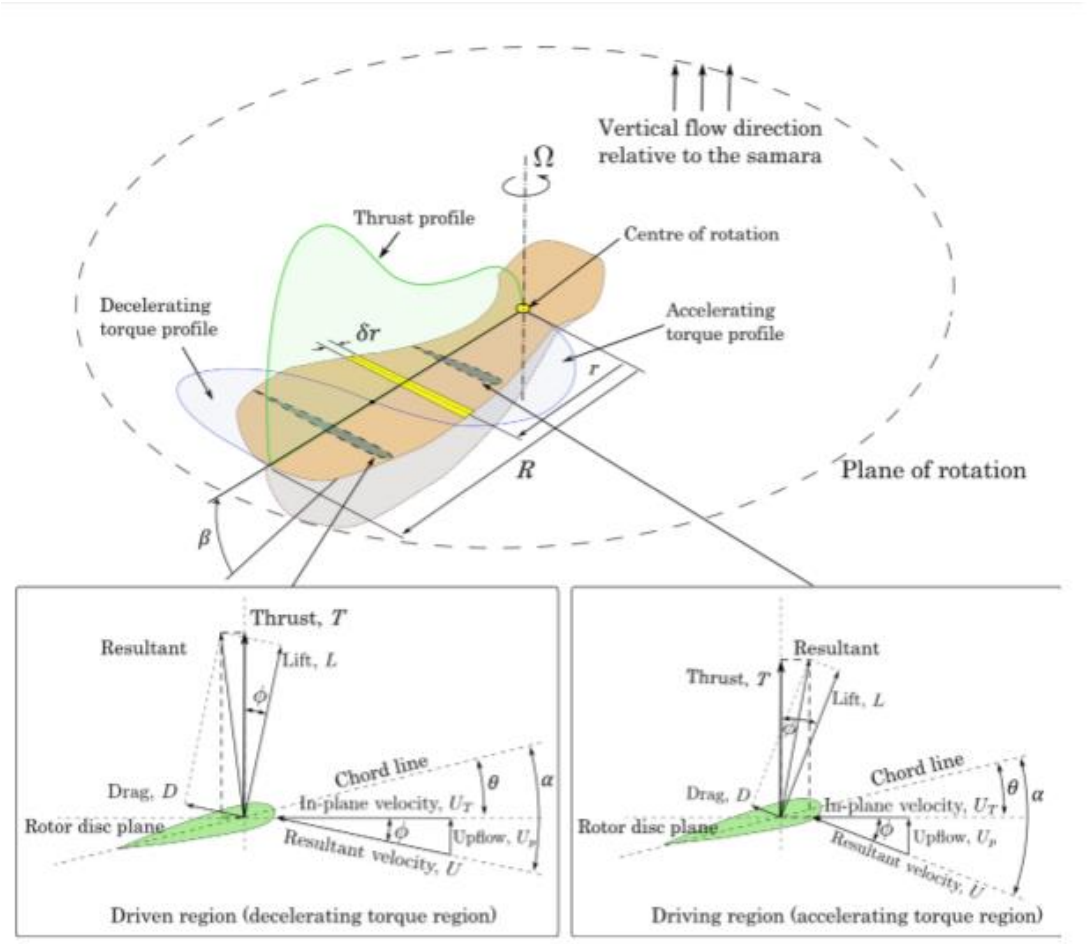

Figure 2 Aerodynamic force components acting on the samara seed blade in both the accelerating and decelerating region (Rezgui D. et al. 2020)

The presented snapshot of the wing during stable flight conditions includes the description of the driven and driving region. The difference in the created torque and thrust between them is a result of different flow conditions and structural properties that vary with the spanwise position. However, stable samara seed flight is a result of a careful balance between these forces. Rezgui D. et al. (2020) build on top of this knowledge and developed three equilibrium conditions that were necessary to achieve such flight

$$\begin{cases} T\cos\beta - T_m = 0 \\ T\cos\beta - Mg = 0 \\ Q = 0 \end{cases} \qquad \begin{matrix} 5.1 \\ 5.2 \\ 5.3 \end{matrix}$$

The first equation in the above system assumes that the thrust generated by a samara seed can be predicted with a momentum analysis (Leishman J.G., 2002). Equation

5.2 describes the relation between the thrust achieved by a samara seed and its weight. When a samara seed achieves a stable flight, it does not accelerate in any vertical direction and therefore its thrust must support its entire weight. Equation 5.3 relates to the generated torque on a samara seed wing. This must be equal to 0, as, during stable flight conditions, the rotational speed is considered to be constant. The torque generated by the whole driving and driven region must cancel out. A system of 3 equilibrium conditions allows to solve for 3 unknowns. 2 of these unknowns are found in the equation that describes the thrust predicted by a momentum analysis

$$T_m = 2\rho A(V_d - v_i)v_i \tag{6}$$

Where ρ and A are the density of air and area of the rotor disc respectively. V_d and v_i are considered to be the 2 unknowns in the code that Rezgui D. et al. (2020) have developed. The last unknown in their code is the rotational speed, ω, of the samara seed. In order to solve for the unknowns, the thrust generated and torque at each radial position had to be described with the unknowns and other inputs that are specified in the code. To solve the system of equilibriums, the overall thrust and torque must be calculated. Rezgui D. et al. (2020) has applied a blade element momentum theory that splits the wing into equally large parts and evaluates aerodynamic forces and therefore thrust, and torque acting on each of these elements. The overall thrust and torque can be achieved by integrating over the span of the blade.

$$\mathrm{T} = \sum_{i=1}^{n} \delta T \cos(\beta) \tag{7}$$

$$\mathrm{Q} = \sum_{i=1}^{n} \delta Q \tag{8}$$

The geometrical relations between the thrust and torque, and the aerodynamic forces that they are composed of are shown in figure 2. Therefore, the thrust and torque at different radial positions will be equal to

$$\delta T = \delta L \cos(\phi) + \delta D \sin(\phi) \tag{9}$$

$$\delta Q = \delta L \sin(\phi) + \delta D \cos(\phi) \tag{10}$$

where ϕ is the local inflow angle. Its value depends on the local flow velocity direction and can be assessed as a relation between the up-flow velocity (U_p) and the in-plane velocity (U_T). Its geometrical relation is shown in figure 2 and therefore is equal to

$$\phi = \tan^{-1}(\frac{U_p}{U_T}) \tag{11}$$

Both equations 9 and 10 include lift and drag forces that must be calculated. With the assumption of two-dimensional steady flow, these two forces can be calculated for each blade element.

$$\delta L = 0.5\rho U^2 c\delta r C_L \eta_{tip} \tag{12}$$

$$\delta D = 0.5\rho U^2 c\delta r C_d \tag{13}$$

U, c, δr, are the incoming flow velocity, average chord of the wing, and local radial distance respectively. The inclusion of η_{tip} term in equation 12 accounts for the tip loss and can be described with

$$\eta_{tip} = \frac{2}{\pi}\cos^{-1} e^{-\frac{1}{2}\left(\frac{1-\frac{\delta r}{R}}{\frac{\delta r}{R}\phi}\right)} \tag{14}$$

Where R is the local blade radius and e is the Euler's number.

The coefficient of lift and drag have already been discussed in the aerodynamic model section of literature review. Rezgui D. et al. (2020) have used equation 3 to calculate it for the model that they have implemented. As angle of attack is included in that equation, the coefficient of lift changes depending on the radial position of the blade part. Therefore, the coefficient of lift will have to be evaluated for each blade element, since the angle of attack is given as

$$\alpha = \theta + \phi \tag{15}$$

where θ is the local elemental pitch angle. This angle is composed of the datum blade pitch angle and the local twist relative to the datum that is simplified to be zero (Rezgui D. Arroyo I. H. and Theunissen R. , 2020). An expression for angle of attack also includes the elemental inflow angle that is described by equation 11. This causes

the angle of attack to change depending on the radial distance from the centre of autorotation. In order to solve the system of equations 5.1,5.2,5.3, the terms that have been described must be expressed with 3 unknowns that are to be solved for. Rezgui D. et al. (2020) have thus described the incoming flow velocity as a combination of in-plane velocity and up-flow velocity.

$$U_T = \omega r \tag{16}$$

$$U_p = (V_d - v_i)\cos(\beta) - \dot{\beta} r \tag{17}$$

where ω, V_d, v_i and $\dot{\beta}$ are rotational speed, descent velocity, downwash velocity blade flapping angle respectively of which the first three terms are solved for by the MATLAB code.

3 Matlab analytical model

3.1 Overview

The core of the Matlab code is based on the blade element theory developed by William Froude (1878). It is used to describe the aerodynamic forces on rotating blades by splitting the wing into small parts. The aerodynamic forces are then evaluated for each part and integrated over the span of the wing to achieve the total lifting force. The samara seed wing has therefore been split into equally large parts to allow for precise calculation of these forces at different spanwise positions. This theory is often combined with momentum theory to produce blade element momentum (BEM) theory. This allows for an approximation of the induced velocity on the disc. The implementation of BEM by Rezgui D. et al. (2020) has been followed to some extent in this study. However, there have been some improvements that will be explained in later parts of this paper. The main differences include the aerodynamic model and the implementation of a structural model.

3.2 Inputs

First, the inputs that are kept constant and samara seed-specific must be specified. Since samara seeds usually operate at low altitudes, it has been assumed that the model will be operating at a see level in accordance with the international standard atmosphere (ISA). Following, the acceleration due to gravity has also been assumed to be equal to that found at sea level.

Parameter	Value
Gravitational acceleration (g)	$9.81\ \frac{m}{s}$
Air density (ρ)	$1.225\ \frac{kg}{m^3}$
Euler's number (e)	2.71828
Mass (M)	0.35 g
Radius (R)	0.0368 m
Root chord (c_r)	0.008 m
Blade pitch angle (θ)	7°

Table 1 MATLAB code inputs that are constant

A more accurate samara seed model is needed to assess the deflections that its wing would undergo. Therefore, the samara seed wing shape has been described with the available resources. Specifically, the wing thickness at different radial and chordwise positions was needed.

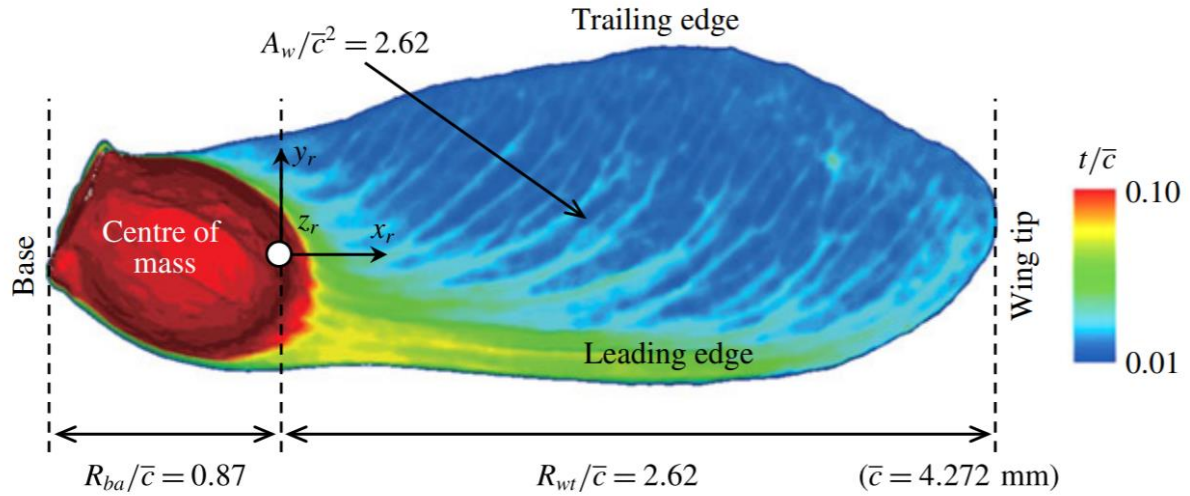

Figure 3 Scanned 3D samara seed model (Acer palmatum). The different colours represent the thickness of the samara seed at that position (Lee I. and Choi H., 2018)

The above figure represents a 3D scanned samara seed where the varying thickness has been expressed as a fraction of the mean chord of the wing. Unfortunately, the exact scan has not been found and this paper's model has been based on this figure. Therefore, some simplifications to the samara seed structure have been made:

- Only the shape of the samara seed wing has been considered
- The 'bottom' surface of the wing has been simplified to be flat
- The leading edge has been assumed to be straight and perpendicular to the chordwise cross-section

- The trailing edge and other edges have been simplified as straight lines
- The thickness of the wing has been split into five different values that are closest to their representative colour on figure 3
- Samara seed is composed of only one material that has the same material properties.

As a result of the above simplifications, the following top view of the wing has been developed.

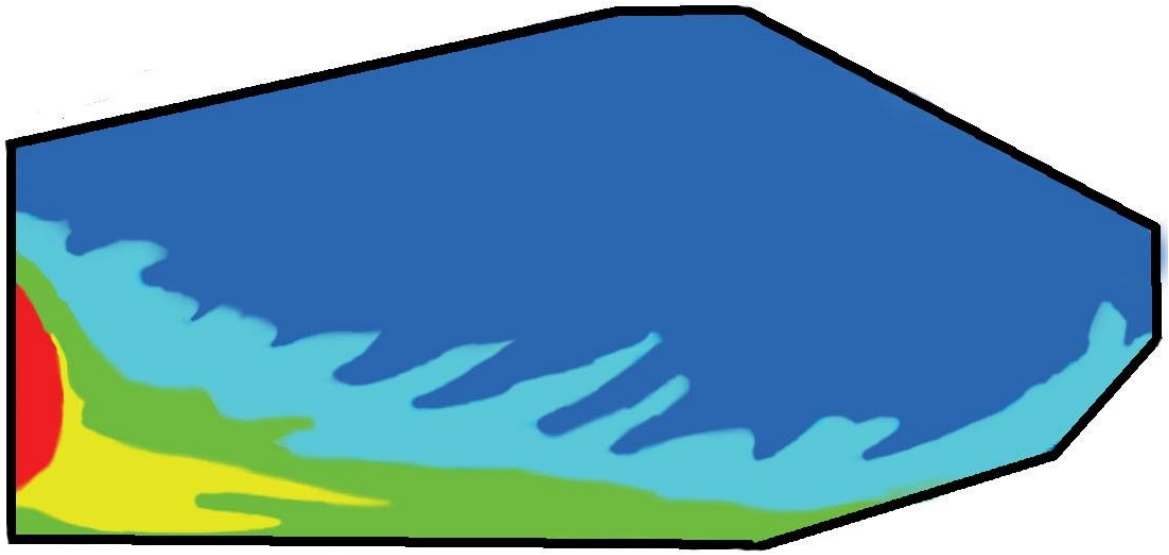

Figure 4 A simplified representation of the samara seed's varying wing thickness

The 5 different colours represent the thickness at different wing positions as a factor of the mean chord. Red, yellow, green, light blue and blue represent 0.1, 0.07, 0.05, 0.025 and 0.01 values respectively. The thickness values have been implemented into the MATLAB code as points at which the corresponding colour value is set. Therefore, figure 4 has been split into 80 equidistant points in the radial direction and 30 similar points in the chordwise direction.

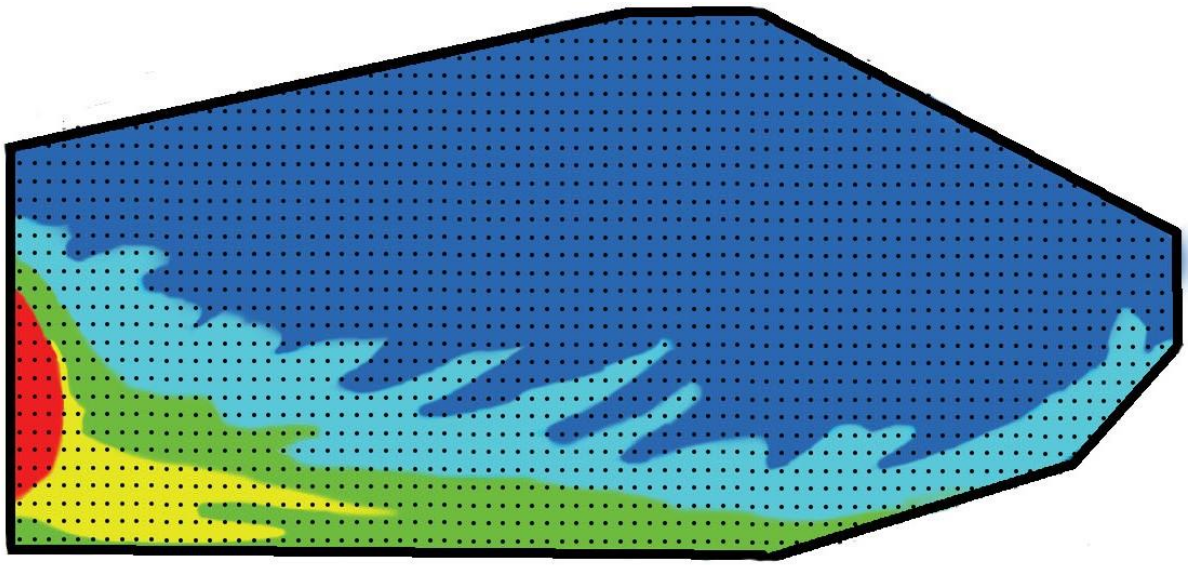

Figure 5 Simplified samara seed wing with positions of the sampling points for the thickness distribution

Additionally, the above figure allowed the description of the chord length distribution with its radial position. This method should provide more accurate results when calculating the achieved lift and drag forces through equations 12 and 13. The Figure below presents the thickness distribution that has been coded accordingly to the figure 5 sampling description and the chord distribution.

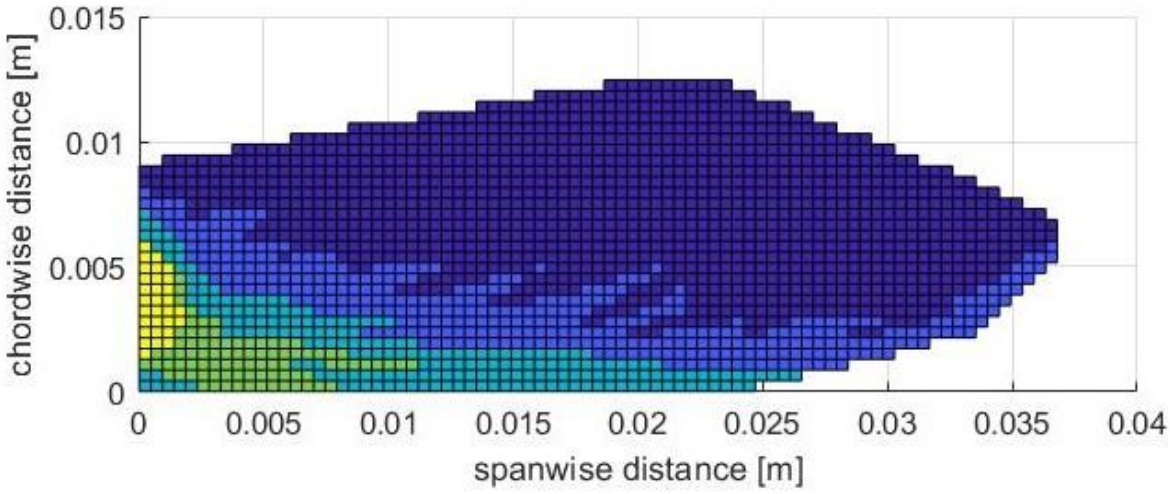

Figure 6 Samara seed thickness distribution coded in Matlab

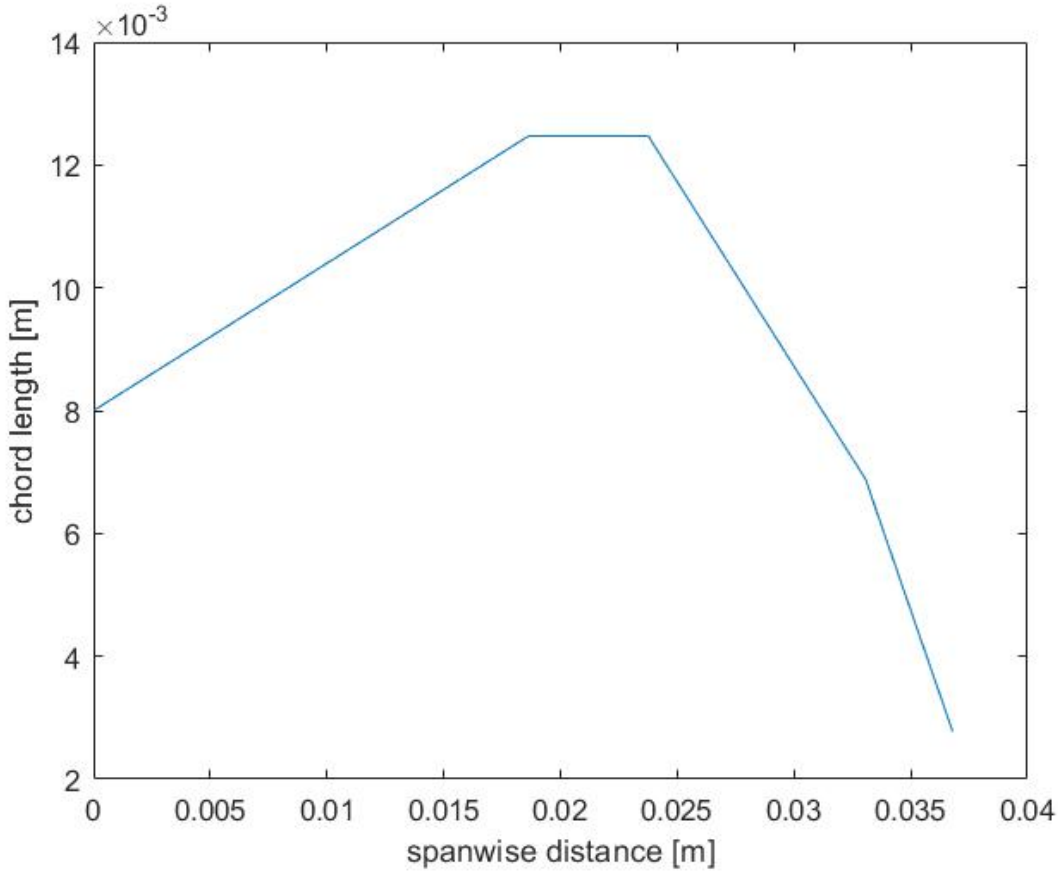

Figure 7 Chord length distribution along the samara seed wing span

3.3 Developed model

Following the BEM theory, the samara seed wing has been split radially into 80 smaller blades at which the aerodynamic forces will be evaluated. The number of parts matches the number of sampling points that have been used for the description of the wing thickness. Along with the constant inputs that have been discussed in the previous section, 4 unknowns are fed into the code as symbolic scalar variables with a function called syms. These variables are descent velocity (V_d), angular velocity (ω), downwash velocity (v_i) and the coning angle (β). They will be used to describe the necessary force balances in order to solve a system of 4 equilibriums and find their values. The 3 equilibriums that have been described by Rezgui D. et al. (2020) and mentioned in equation 5, will be used along with a fourth one that has been developed in order to solve for the coning angle that is specific to every samara seed. In order to do so, a fourth equilibrium that describes a stable samara seed flight had to be found. Since samara seed flight is a rotational motion that operates at some coning angle relative to the datum plate, it has been deducted that an equilibrium between

the centrifugal and created aerodynamic force must be present. An equation that describes the centrifugal force is presented below:

$$F_c = M\omega^2\delta r \tag{18}$$

The above equation changes depending on the radial distance from the centre of rotation, therefore this force can be assessed at each blade part of the wing. Therefore, a mass distribution that depends on the radial position had to be found. With the implementation of the thickness distribution and an assumption of the samara seed being composed of only one material, the material density can be assumed to be constant. Therefore, by summing the thickness of all points ($\sum thickness$), mass proportions, $mass_p(i)$, can be found at each radial position.

$$mass_p(i) = \frac{thickness(i)}{\sum thickness\,(i)} \tag{19}$$

where $thickness(i) = \sum_{j=1}^{30} thickness_i\,(j)$ and $\sum thickness(i) = \sum_{i=1}^{80} thickness(i)$.

However, samara seed centrifugal force is not only created by the rotating wing, but also by the seed that rotates on the opposite side of the centre of rotation. The centre of rotation has been assumed to coincide with the centre of gravity. As a result, half of the samara seed mass is simplified to be located on both sides. Therefore, the centrifugal force acting on each blade part is given by the following equation:

$$F_{cr}(i) = 0.5 * M * mass_p(i) * \omega^2 * r(i) \tag{20}$$

where $r(i)$ is the radial distance to the centre of rotation at each blade element out of 80. Furthermore, the centrifugal force acting on the seed can be described with

$$F_{cs} = 0.5 * M * \omega^2 * 0.15822R \tag{21}$$

Where the value of $0.15822R$ is found as half the distance from the beginning of the wing to the end of the seed based on the proportions depicted in figure 3. To create an equilibrium of forces that will allow to find the coning angle, there needs to be another force acting in the same direction as the centrifugal force. This force is the result of the thrust force produced by each blade element that is composed of vertical

and in-plane components. The in-plane component is the force that acts in the same direction as centrifugal forces and can be expressed by:

$$F_{cT} = \sum_{i=1}^{n} \delta T \sin(\beta) \tag{22}$$

where δT is described by equation 9. This allows to form an additional fourth equilibrium that describes the steady samara seed flight. The system of equilibriums for this MATLAB code is therefore given by:

$$\begin{cases} T\cos\beta - T_m = 0 \\ T\cos\beta - Mg = 0 \\ Q = 0 \\ \sum_{i=1}^{80} F_{cr}(i) - F_{cT} - F_{cs} = 0 \end{cases} \tag{23}$$

The rest of the kinematic model that has been implemented in this model is very similar to the model developed by Rezgui D. et al. (2020), however, some changes have been made. Most of the differences in this model can be found in the aerodynamic description of how the samara seed creates lift and drag forces. The primary change is made in the derivation of the coefficient of lift that is applied in equation 12. The method used to describe this variable has been found in the paper written by Nabawy MRA and Crowther WJ. (2017). According to the normal force model for samara seeds that they have developed, the 2D coefficient of lift can be expressed by equation 4. However, for the purposes of this paper, a 3D coefficient of lift is needed. According to MRA and Crowther WJ. (2017), this coefficient of lift is also driven by the same rules that apply to the 2D case.

$$C_L = C_{l\alpha,3D} \sin\alpha \cos\alpha \tag{24}$$

The above equation describes the 3D lift coefficient where $C_{L\alpha,3D}$ is the 3D lift curve slope as opposed to the 2D lift curve slope that is used in the two-dimensional case. One of the expressions for the three-dimensional lift curve slope, that has been developed and can be found in literature, is explained by the Prandtl's lifting line theory. Its equation can be found in a paper written by Nabawy MRA and Crowther WJ. (2014B):

$$C_{l\alpha,3D} = \frac{C_{l\alpha,2D}}{E + \frac{kl_{L\alpha,2D}}{\pi AR}} \tag{25}$$

where E, k, and AR are the edge correction, 'k-factor', and the aspect ratio, respectively. The 2D lift curve slope for an aerofoil that is simplified to be a flat plate has a theoretical value of $2\pi\ rad^{-1}$. However, its value is influenced by the Reynolds value at which the wing operates. Since samara seeds operate at a low Reynolds value, Okamoto M. et al. (1996) have found the lift curve slope to be equal to around 4.9 rad^{-1}. This value will be used in this study to assure accuracy. The edge correction factor has been introduced as a correction to the lifting line theory for the chord of an infinite wing by Jones RT. (1941). It brings the lift curve slope value closer to the values predicted by the conducted experiments. The edge correction value has been assessed with respect to the table presented below.

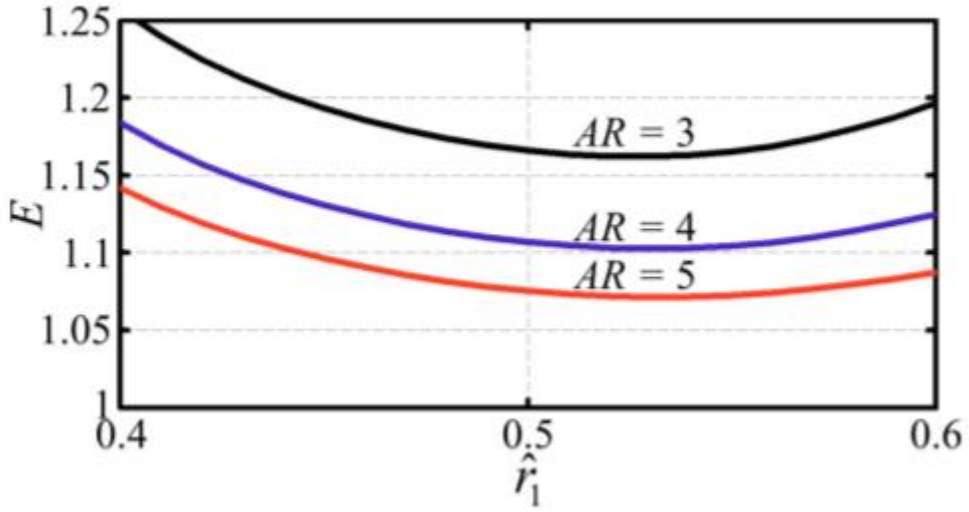

Figure 8 Edge correction variation factor with respect to the aspect ratio and centroid location (Nabawy MRA, Crowther WJ, 2015)

To account for the differences that appear in the 3D treatment of flow, the induced power factor, k, has been introduced into the equation. Nabawy MRA and Crowther WJ. (2014A) have described the components that compose the parameter k in samara seed wings.

$$k = k_{ind} k_{tip} k_{flap} \tag{26}$$

where

$$k_{ind} = \frac{2\int_0^1 (v_i(\hat{r}))^3 \hat{r} d\hat{r}}{\left(\sqrt{2\int_0^1 (v_i(\hat{r}))^2 \hat{r} d\hat{r}}\right)^3} \tag{27}$$

$$k_{tip} = \frac{1}{B} \tag{28}$$

$$k_{flap} = \sqrt{\frac{\pi}{\Phi}} \tag{29}$$

One of the contributors to that variable is the k_{ind} which accounts for a non-uniform downwash distribution since the 2D case assumes it to be uniform. To calculate its value, the downwash velocity distribution, $v_i(\hat{r})$, is needed where $\hat{r} = r/R$. Nabawy MRA and Crowther WJ. (2014A) discuss how such downwash velocity distribution can be achieved and have calculated k_{ind} for wings of various insects. Due to the similarity of insect and samara seed wings, and small differences between the values calculated for each insect by Nabawy MRA and Crowther WJ. (2014A), the value of k_{ind} will be taken as their mean, which is 1.18. The k_{tip} factor considers tip losses where B is the non-dimensional effective radius. Nabawy MRA and Crowther WJ. (2014A) have used Prandtl theory for tip loss correction in rotors with N_b number of blades.

$$B = \frac{R_e}{R} = 1 - \left(\left(\frac{2\ln 2}{N_b}\right)\frac{\lambda}{\sqrt{1+\lambda^2}}\right) \tag{30}$$

λ is the ratio of the induced downwash to the wing tip velocity and R_e is the effective blade radius. This theory assumes that, due to the aerodynamic losses at the tip, the effective radius gets reduced. While this is a correct description of tip losses in samara seeds, the tip loss factor has already been accounted for by equation 14. Therefore, to not double count for this effect, the k_{tip} value has been simplified to be 1. Nabawy MRA and Crowther WJ. (2014A) have included a third contributor, k_{flap}, in order to account for the losses due to the flapping in the insect flight. They simplified this effect to cause a reduction in the effective disc area, which caused an increase in the

disc loading and induced velocity. However, this effect is only relevant to a flight that uses flapping to produce lift. Despite the similarities, between the insect and samara seed wings, k_{flap} can be considered irrelevant in this model. Therefore, the induced power factor will be expressed by

$$k = k_{ind} = 1.18 \tag{31}$$

for the purposes of this model. Finally, coming back to equation 25, the 3D lift curve slope coefficient can be calculated by inputting the factors that have been described above.

With all the differences between the Matlab code developed in this paper and the one created by Rezgui D et al. (2020) explained, the described model can evaluate for the four unknowns. A function called vpasolve has been used to solve the system of equations described in 23. After the code evaluation of the aerodynamic and kinematic equations, the system of equilibriums is described by these four variables. A function called vpasolve has been used to solve this system and output these unknowns.

3.4 Second iteration

The first part of the Matlab model has focused on acquiring the correct performance values for a specific samara seed structure. However, this structure is assumed to be inflexible in that model. The aim of this paper is to gain some insight into how various structural properties could influence the samara seed performance, therefore a model that considers the flexibility of the structure is necessary. One way to measure the structural flexibility of an object is to calculate its deflection under certain loads. The deflection of the samara seed wing will be considered in this section and its influence will be measured. However, only the vertical deflection of a wing depending on its radial position will be considered. Any deflection changes at different chordwise positions of a specific radial position will be restricted. Additionally, the wing has been assumed to be a beam under a varying load. This varying load is caused by the created aerodynamic forces. The first iteration of the process has supplied the values for the second iteration and forces at each radial position have been calculated for the achieved unknowns. The expressions for the deflections (δ) of a beam under load can be found below

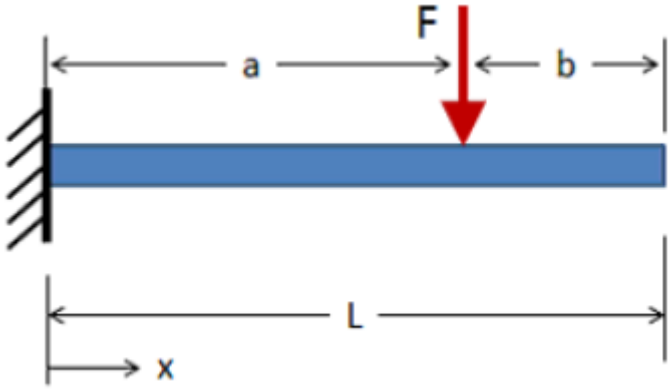

Figure 9 Beam deflections schematic diagram (https://mechanicalc.com/reference/beam-deflection-tables)

$$\delta = -\frac{Fx^2}{6EI}(3a - x) \quad \text{for} \quad 0 \leq x \leq a \tag{32}$$

$$\delta = -\frac{Fa^2}{6EI}(3x - a) \quad \text{for} \quad a \leq x \leq L \tag{33}$$

where F is the force acting at some point a of the beam and x is the position at which deflection is evaluated. E is the Young's modulus of the material that the beam is composed of and I is the second moment of area of the beam. In order to implement this theory into the developed Matlab model, the second moment of area of the samara seed wing has to be found. However, the structural description implemented in the inputs section includes different wing cross-sections at each radial position. This will lead to a different second moment of area of each blade element. The chordwise cross-section at each radial position has been assumed to be composed of rectangles for simplicity. Since the bottom surface of the samara seed wing has been assumed to be flat, the height of each of these rectangles is equal to the thickness at the specified point. Therefore, the second moment of area can be assessed against one axis at which the base of each rectangle lies. The second moment of area of a rectangle with respect to an axis passing through its base is specified by:

$$I = \frac{bh^3}{3} \tag{34}$$

Where b is the width of the rectangle and h is its height. To assess the area moment of inertia at each radial position, each one of these rectangles can be summed together. The width of one rectangle has been assumed to be equal to the maximum

chord over the number of chordwise sampling points. Therefore, the equation for the second moment of area takes the form of

$$I(i) = \sum_{j=1}^{30} \frac{b(h(j))^3}{3} \tag{35}$$

Along with the second moment of area, Young's modulus is needed in order to assess wing deflection. It has been discussed that, for the purposes of this model, a samara seed is considered to be built of only one material. Along with the same density at each point, Young's modulus will take the same value as well. The force acting at each radial position normal to the wing is the aerodynamic force of thrust. Furthermore, this force is the reason for the beam deflection. However, there is also the force of gravity that must be accounted for. It can be described as

$$F_g(i) = 0.5 * mass * mass_p(i) * g * \cos(\beta) \tag{36}$$

where term $\cos(\beta)$ assures that this force acts normal to the surface. Additionally, the beam deflection equation must be modified to calculate the total deflection caused at a specific position due to forces acting at other radial positions. The sum of the deflections at some radial position is given by:

$$\delta(i) = \delta_1(i) + \delta_2(i) \tag{37}$$

where

$$\delta_1(i) = \sum_{n=1}^{i-1} \left(\frac{(T(n) - F_g(n)) * (r(n))^2}{6 * E * I(i)} (3r(i) - r(n)) \right) \quad \text{for} \quad 0 \le r(n) < r(i) \tag{38}$$

$$\delta_2(i) = \sum_{n=i}^{80} \left(\frac{(T(n) - F_g(n)) * (r(i))^2}{6 * E * I(i)} (3r(n) - r(i)) \right) \quad \text{for} \quad r(i) \le r(n) \le R \tag{39}$$

The $T(n)$ is the thrust normal to the wing achieved at each radial position. It has been described by equation 9. The wing deflection will have an influence on the performance of the samara seed through a changing coning angle. The calculated deflections can be used to achieve coning angle at each radial position. The change in the coning angle due to the deflections is given by:

$$\beta_\delta(i) = \tan^{-1}\left(\frac{\delta(i)}{r(i)}\right) \tag{40}$$

$$\beta(i) = \beta + \beta_\delta(i) \tag{41}$$

The second iteration of the Matlab code is based on the new coning angle value. This value transforms into a vector of values in the second iteration based on the predicted deflections of the wing. Therefore, the influence of the structural flexibility can be assessed by solving the system of equilibriums. As the coning angle is a set input, there will be only three unknowns during the second iteration process. Thus, only the first three equilibriums from equation 23 will be needed. All the other inputs and constants are kept constant in relation to the first iteration. This method will supply 3 variables that are measures of samara seed flight performance. With the second iteration process run for different values of Young's modulus, one can assess how the performance of samara seed will change depending on the material flexibility.

4 Results and Discussion

4.1 First iteration results

The aim of the first part of the code was to acquire performance parameters for the specified samara seed inputs. The achieved unknowns have been presented below.

Descent velocity, V_d	$1.402\ \frac{m}{s}$
Angular velocity, ω	$30.142\ \frac{Rad}{s}$
Induced velocity, v_i	$1.103\ \frac{m}{s}$
Coning angle, β	$0.349\ Rad$

Tabela 1 First iteration results

The achieved values can be assessed against available data in the literature. Rezgui D et al. (2020) have performed an experiment in a vertical wind tunnel, where they recorded the samara seed flight performance parameters at different velocities of vertical flow. The data that they have achieved for the angular velocity at different descent velocities have been presented below.

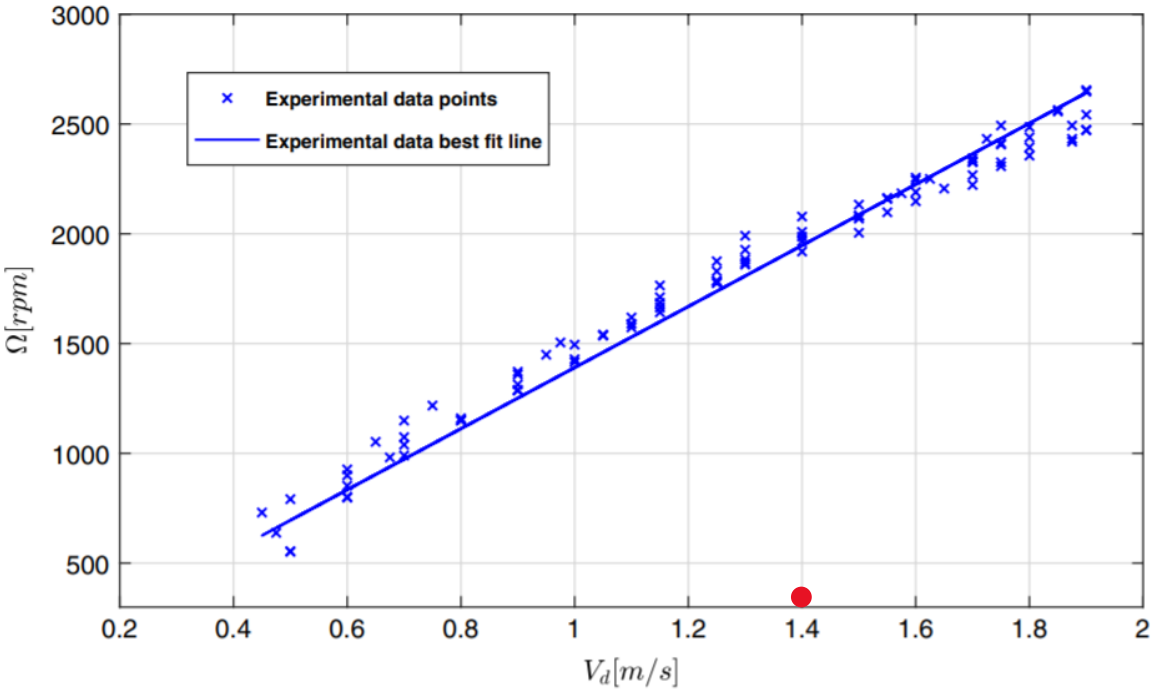

Figure 10 Rotational speed dependance on the descent velocity based on experimental findings by Rezgui D. et al. (2020)

The values acquired from the model developed in this paper were approximately marked on the above graph by a red dot. It is apparent that the value of the angular velocity does not correspond with the measured experimental data. However, the experiment made by Rezgui D. et al. (2020) had some restrictions. The experiment did not allow to measure the coning angle correctly, as a string that was mounted to the samara seed centre of gravity could have restricted some movement. Rezgui D. et al. (2020) have commented on that observation and concluded that the string could have made it impossible for the samara seed to achieve its true free fall coning angle. Furthermore, the code does output a descent velocity that lies in a possible range. Additionally, the coning angle that has been calculated is equal to around 20° . This value is supported by a free-fall experiment done by Lee Sujin et al. (2014) where the coning angle of a samara seed has been estimated to be 19.4 degrees. They have also acquired the value of the descent velocity which was approximated to be 1.26 $\frac{m}{s}$. This is relatively close to the value that has been calculated by the Matlab code. Even though the samara seed structural constants are different, when compared with the inputs used in this paper, in the experiment done by Lee Sujin et al. (2014), they do not differ greatly. It supports the statement that the descent velocity and coning angle value lie in a possible range of correct values. The Matlab code has been explored for

errors, however, no errors were found and the data available in the literature it suggests that the angular velocity predicted by the coded model might not be correct.

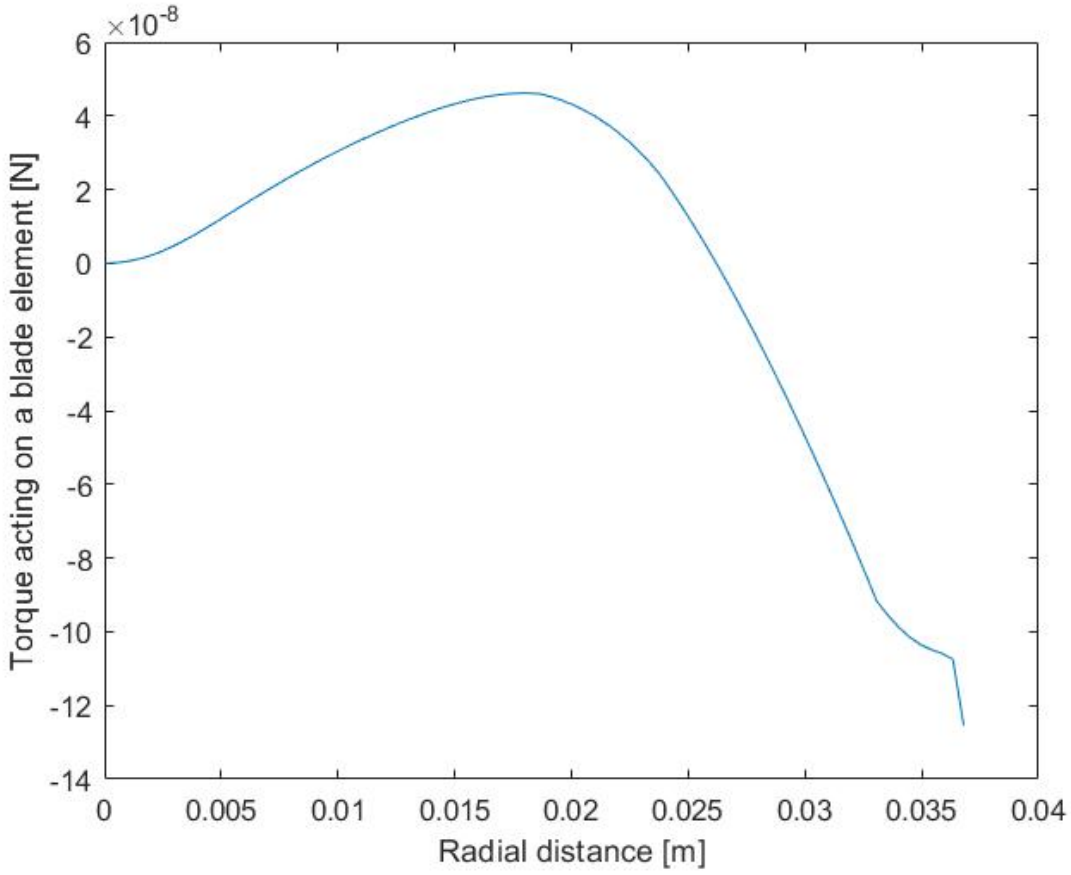

Figure 11 Varying torque created with radial position of a blade element

The above graph represents the torque created with respect to the distance from the centre of rotation. As predicted by figure 2, the wing should be split into two regions. The predicted torque agrees with that theory and even though torque takes positive values for most of the portion of the wing, the average absolute value of the torque in the driven region is lower than that of the driving region. This indicates that the requirement of the total torque being equal to 0 should be met.

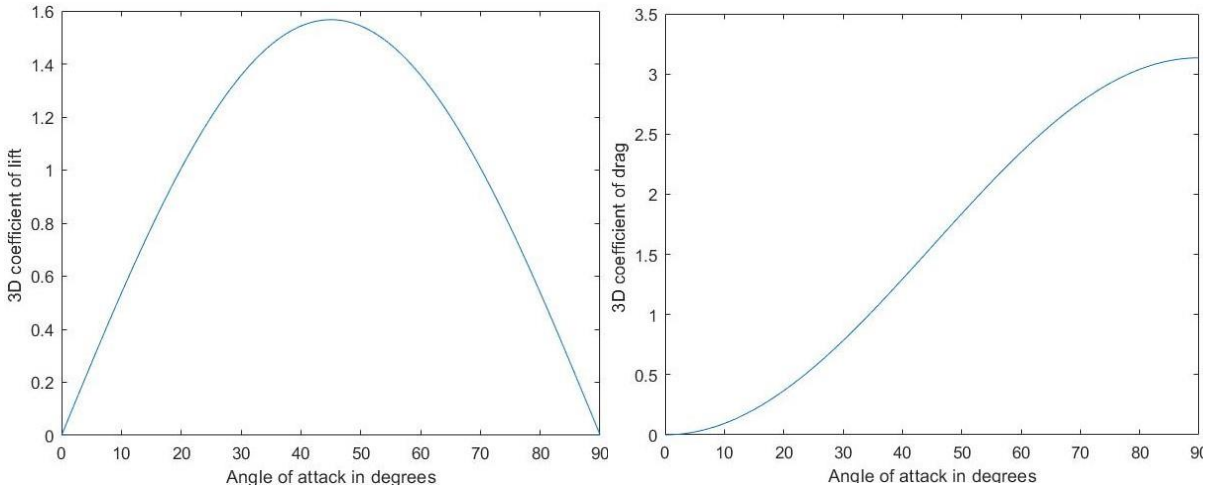

Figure 12 3D coefficient of lift and drag with respect to the angle of attack, where the 3D lift curve slope is equal to 3.13

Both three-dimensional coefficients of lift and drag correspond to the normal force theory developed by Nabawy MRA and Crowther WJ (2017). According to that theory, the coefficient of lift should decrease to 0 at 90 degrees angle of attack due to a geometric correction introduced by Nabawy MRA and Crowther WJ (2017). It confirms the validity of above graphs.

4.2 Deflections

The first iteration of the Matlab code assumed that the samara seed is an inflexible wing. It allowed to calculate the naturally occurring coning angle of the samara seed that doesn't consider any deformation to the wing. However, every material deflects due to even the smallest of forces. It may not always be visible or cause any relevant performance changes, but it must be considered in engineering of any kind. This results section will explore the deflections of the samara seed wing during its flight. Mass is one of the material properties that could be addressed during the samara seed drone design stage. As samara seed flight is a careful balance between the inertia and aerodynamic forces, mass can be a very important factor while designing such a vehicle. It is included in one of the equilibrium equations, 5.2, as the thrust created samara seed wing has to support the whole weight. Additionally, it also influences the deflection of the wing since the wing's mass will drag it in a downward direction.

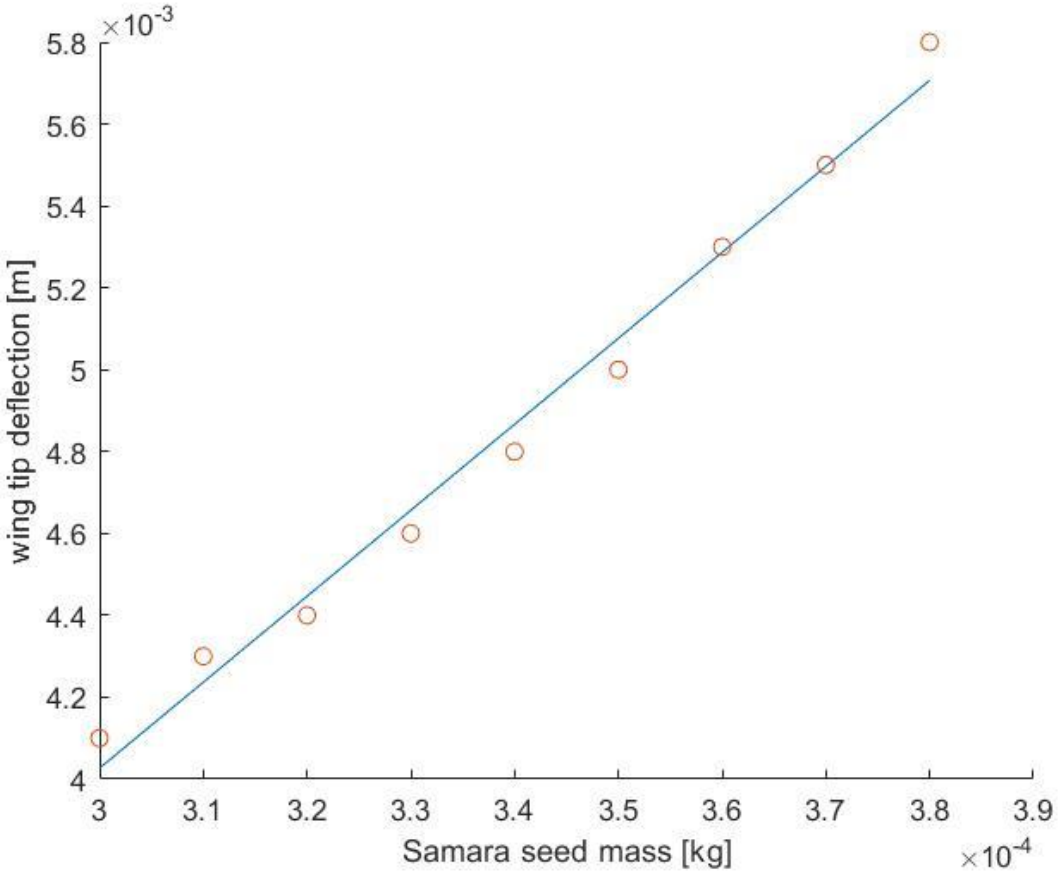

Figure 13 Wing tip deflection relative to samara seed mass for Young's modulus = 1GPa

Results obtained on the graph above indicate that the wing tip deflection increases with an increase in samara seed mass. Referring back to equations 38 and 39, the deflection of the samara seed relates to the resultant of the force of gravity component and Thrust force acting on a blade element. Only these two forces influence the values calculated by this equation as all the other variables are constant for the case presented in figure 13. Following this reasoning, this indicates that an increase in mass of the samara seed increases the thrust it generates. Moreover, the increase in the thrust force causes larger deflection as the increase in the force of gravity normal to the wing is relatively smaller.

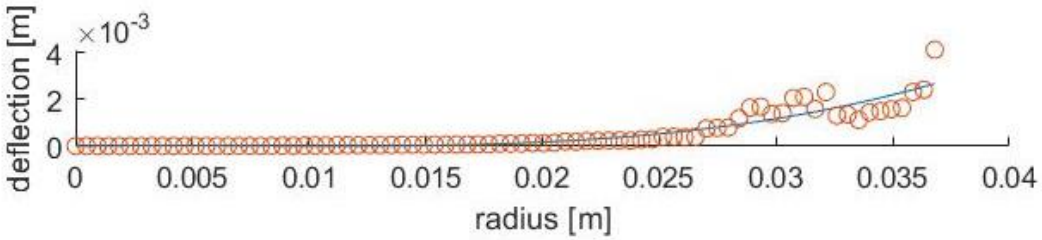

*Figure 14 Samara seed wing deflection for E = 1*10^9*

The graph above presents the deflection of the wing relative to its blade element position for a samara seed mass of 0.35 grams. Each circle represents one blade element and a line has been drawn, using a third-order polynomial, to assess the best fit between them. The application of equations 38 and 39 predicts the deflection of each of these elements, with the assumption of the wing behaving similarly to a beam. There is a decrease in the deflection after the radial position of around 0.0323 m. This might be a result of a varying thickness of the wing. Figure 6 shows that after that point there appears to be an increase in the thickness of a few sampling points. Therefore, an increase in the second moment of area might have occurred. Accordingly, a higher area moment of inertia would resist bending more efficiently. Additionally, according to the plot below.

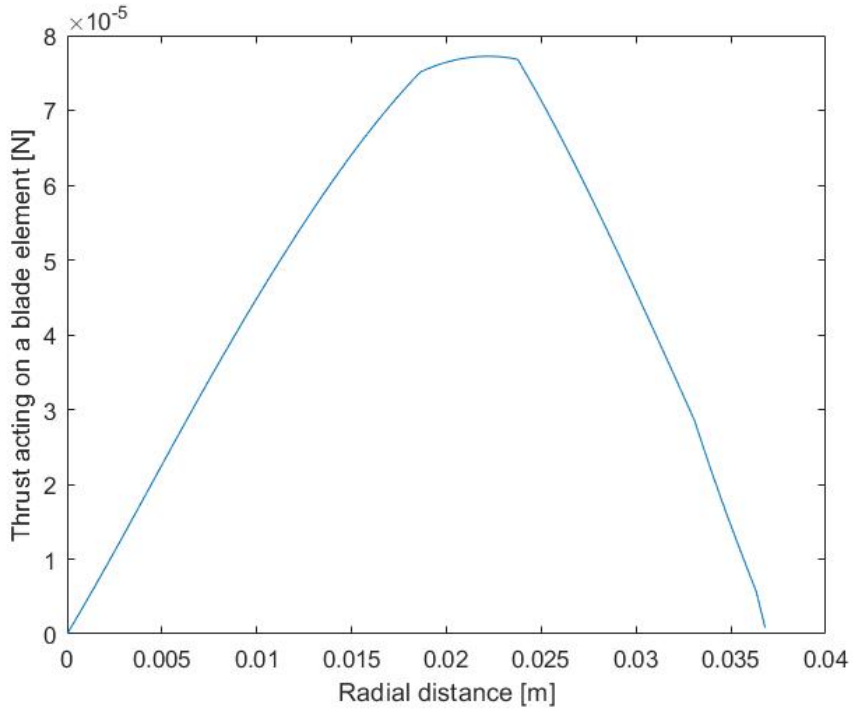

Figure 15 Thrust created by a blade element normal to the wing with respect to the local radial distance

the thrust created by each blade element starts to decrease at around 0.0235 m of radial distance. Thrust is the thrust that causes the beam to deflect upwards. Therefore, the combination of these two variables that decrease with the radial position might account for the sudden decrease in the deflection. After the decrease, the deflection seems to follow the same trendline as before.

By analysing equations 38 and 39 yet again, it can be concluded that the samara seed deflection increases with a decreasing Young's Modulus. Comparison of the graph below

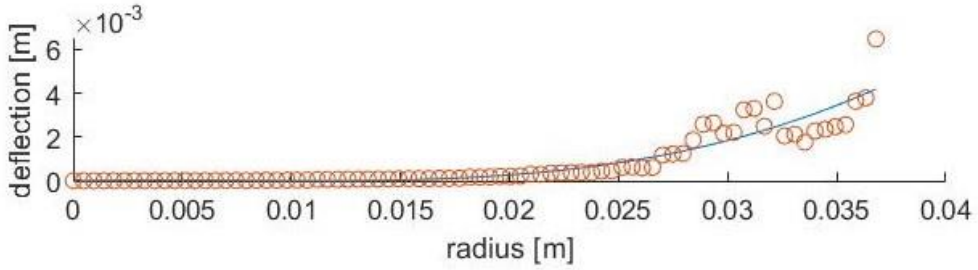

Figure 16 Samara seed wing deflection for E = 0.9GPa

with figure 14 clearly shows that this is true for the Matlab model. The relative changes in values of samara seed wing deflections between each other have increased slightly as the circles lie further away from the best fit line. This is due to the decreased Young's Modulus, which provides less resistance to bending.

4.3 Influence on performance

A clearer insight into how the deflection of the samara seed wing was influenced by the initial inputs has been achieved in the previous section. Additionally, the effect of the material density on the wing deflections has been assessed. While this partly satisfies the aim of this paper, by providing how the structural properties can influence samara seed flight, a further explanation on how its performance differs is needed. One of the fundamental material properties is the Young's modulus which is one of the most influential parameters when considering a material for a design. As has been described in the introduction, this paper's aim is to provide more insight into how the material selection can influence samara seed performance. The developed analytical model has thus been run for a range of Young's modulus values.

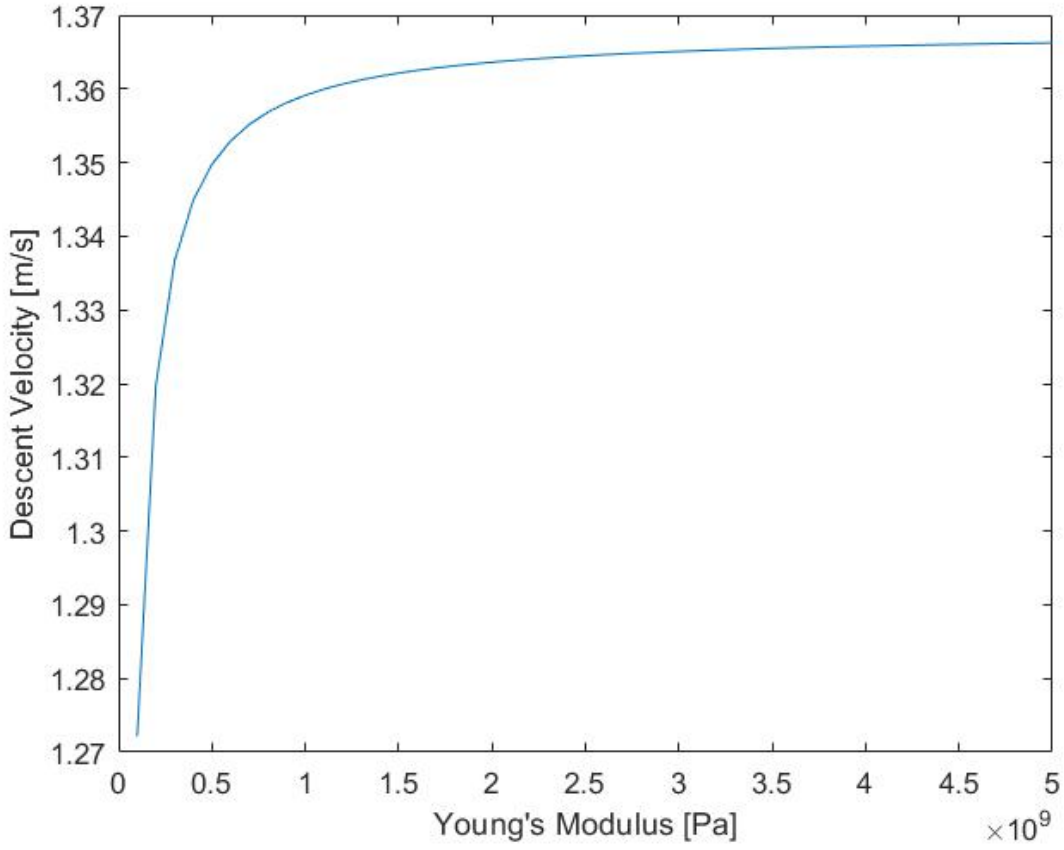

Figure 17 Variation of samara seed descend velocity with Young's modulus

The above graph represents how one of the most fundamental samara seed performance parameters, V_d, depending on the material's Young's modulus. The descent velocity clearly decreases with a decrease in E. The descent velocity seems to approach a certain value as the Young's Modulus increases to infinity. During the first iteration process, an assumption has been made that the wing is inflexible and therefore it could not deflect. It physically means that it had an infinite resistance to a bending moment. This corresponds to the Young's modulus value of infinity as it is a measure of a material's ability to oppose bending moment. Extending this theory to figure 17, it can be concluded that the descent velocity value that the graph approaches at infinite Young's modulus is the value that has been calculated during the first iteration process, 1.402 $\frac{m}{s}$.

On the other hand, the graph also approaches the lowest descent velocity as E gets closer to the value of 0. This is physically impossible in real life, as such flexible material would not be capable of sustaining a rotational flight or opposing deflection due to the created forces. Moreover, the steep decrease in the descent velocity value after

Young's modulus value of around 0.8 must indicate that there are some limitations to the created model, where it fails. Nevertheless, the above graph represents a relationship between the descent velocity and Young's modulus. It provides insight into which material properties to look for when designing a samara seed drone that needs to have the slowest descent velocity. This could be advantageous in a helicopter flight as described at the beginning of this paper. However, this model cannot predict when a material would become overly flexible and thus, unable to autorotate.

Another material property considered during this study is the material density. Figure 13 has described its relation with respect to the wing deflection. However the descent velocity has been also assessed against the varying mass of the samara seed in order to provide a more clear measure.

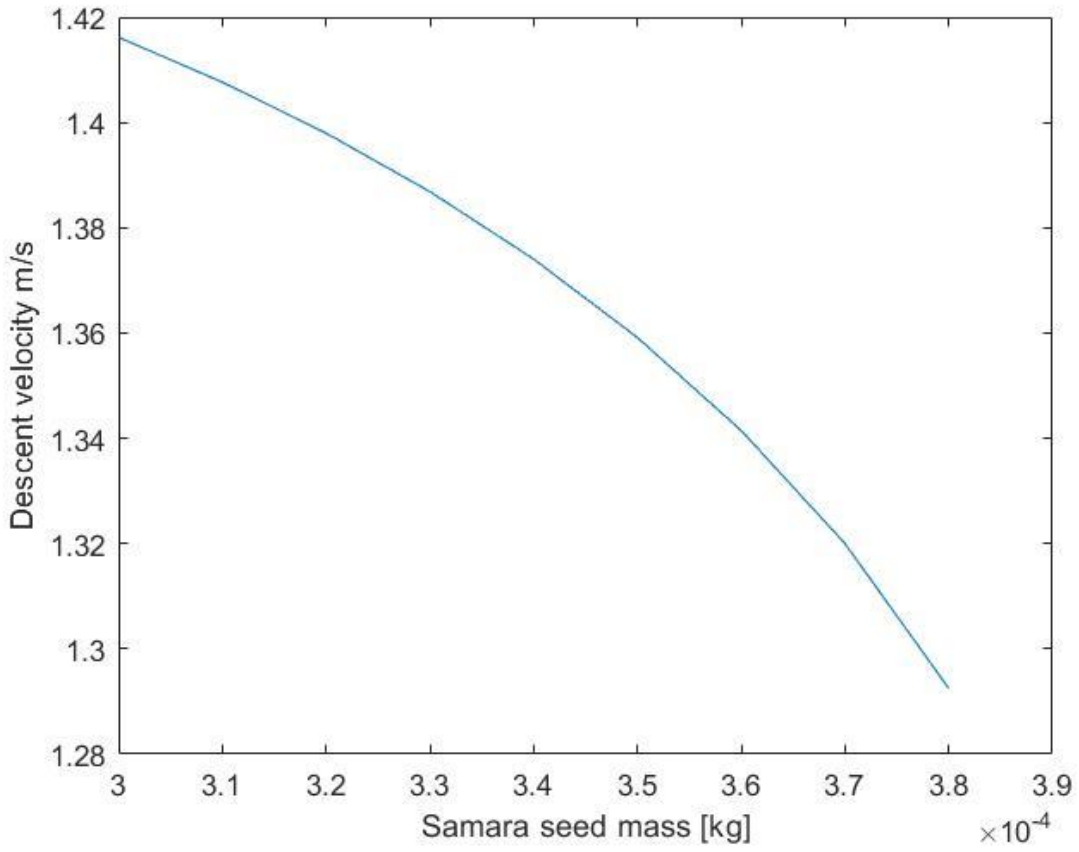

*Figure 18 Descent velocity with relation to the samara seed mass for E = 1*10^9*

As the thickness distribution of the samara seed wing does not change, for the total mass to increase, the material of which it is composed must become denser. Therefore, the above figure presents the relation between descent velocity and material density. It is clear that V_d decreases with increasing density. Thus, according to the

developed model, a denser material will perform better if the aim is to achieve a slower descent. However, this relation cannot be applied to masses that would not allow for the self-autorotation. The depicted fragment of discussed relation will only apply to some range of masses for s specific samara seed structure. There must be a point at which this theory will provide results that are physically impossible, same as in figure 17.

5 Conclusions

The results of the developed model do not show agreement in all aspects when compared with the data available in literature. However, certain performance parameters lie in a possible range and could be correct. The developed model has been checked for incorrect assumptions and improperly developed equations, however no error has been found. It has been deemed that with some values lying in a possible range of correct values, the model described in this paper is accurate to some extent. Furthermore, this should have allowed to capture the relations of structural properties' influence on the samara seed performance. While the exact values might not be correct for calculated variables, the trends that have been shown in the results should still be applicable. It has been concluded that the descent velocity of the samara seed should decrease for lower values of Young's modulus. Additionally, an increase in material density can also provide a slower descent. The aim of the paper was to find a relation between structural properties and their influence on samara seed performance in order to provide some insight into the design of similar artificial vehicles. Based on the findings presented in this paper, the denser and weaker (in terms of Youngs modulus) the material is, the slower the descent velocity of such vehicle will be. Nonetheless, it is apparent that there are some limitations to the developed model and the results become incorrect at some point as they simply become physically impossible. The exact points at which these findings fail to satisfy the requirements for the samara seed autorotation have not been found. A further research into this area is needed to assess the validity of the developed model more accurately and consider other aspects of structural influence on the flight performance.

6 Recomendations

An analytical model for the prediction of samara seed performance under different material properties have been developed in this paper. However, the methods used have only been validated against available literature and they have not showed a good match. An experimental approach which would provide a better benchmark against which the results of this analytical model could be measured is needed. Samara seeds of same shapes could be 3D printed, where each one would have different material properties, i.e., Young's modulus or material density. Then, they could be tested in a free fall experiment to collect the performance parameters that this model predicts. Additionally, with the insights collected from such experiment, the points at which the developed model would fail to correctly describe the flight could be found. This could either include finding an expression for a point at which the model fails or a specific value for the Young's modulus and material density that would be only applicable to a studied samara seed. Such research would provide further insight into the topic at hand and could help develop an improved model which would be more accurate.

Another direction for further research would be to assess the samara seed flexibility not only in the spanwise direction, but also chordwise. Additionally, a more accurate thickness distribution could be acquired by 3D scanning a real samara seed for such a study. It would assure that the simplifications that have been made in the inputs section wouldn't need to be made. Thus a more accurate model for the samara seed structural influence on its performance could be created. Such a study would have potential to yield different results than the results that have been achieved in this study.

References

Nabawy MRA, Crowther WJ. 2017 The role of the leading-edge vortex in lift augmentation of steadily revolving wings: a change in perspective. J. R. Soc. Interface 14: 20170159. http://dx.doi.org/10.1098/rsif.2017.0159

Rezgui, D., Arroyo, I. H. and Theunissen, R. (2020) "Model for sectional leading-edge vortex lift for the prediction of rotating samara seeds performance," *The Aeronautical Journal*. Cambridge University Press, 124(1278), pp. 1236–1261. https://doi.org/10.1017/aer.2020.25

Nabawy MRA, Crowther WJ. 2014A On the quasi-steady aerodynamics of normal hovering flight part I: the induced power factor. J. R. Soc. Interface 11: 20131196. http://dx.doi.org/10.1098/rsif.2013.1196

Nabawy MRA, Crowther WJ. 2014B On the quasi-steady aerodynamics of normal hovering flight part II: model implementation and evaluation. J. R. Soc. Interface 11: 20131197. http://dx.doi.org/10.1098/rsif.2013.1197

POLHAMUS, E.C. A concept of the vortex lift of sharp-edge delta wings based on a leadingedge-suction analogy, NASA-TN D-3767, NASA Langley Research Center, Hampton, VA, US, 1966.

Nabawy MRA, Crowthe WJ (2015) A Quasi-Steady Lifting Line Theory for Insect-Like Hovering Flight. PLoS ONE 10(8): e0134972. doi:10.1371/journal.pone.0134972

Lee, I. and Choi, H. (2018) "Scaling law for the lift force of autorotating falling seeds at terminal velocity," *Journal of Fluid Mechanics*. Cambridge University Press, 835, pp. 406–420. doi: 10.1017/jfm.2017.746.

Okamoto M, Yasuda K, Azuma A. Aerodynamic characteristics of the wings and body of a dragonfly. J Exp Biol. 1996;199(Pt 2):281-94. doi: 10.1242/jeb.199.2.281. PMID: 9317808.

Jones RT. 1941 Correction of the lifting line theory for the effect of the chord. NACA Technical Note 817

Evan R Ulrich, Darryll J Pines and J Sean Humbert, 2010, From falling to flying: the path to powered flight of a robotic samara nano air vehicle, Bioinspir. Biomim. *5,* doi:10.1088/1748-3182/5/4/045009

Azuma, A. and Okuno, Y. (1987) Flight of a Samara, Alsomitra macrocarpa. Journal of Theoretical Biology, 129, 263-274. https://doi.org/10.1016/S0022-5193(87)80001-2

S. K. H. Win, L. S. T. Win, D. Sufiyan, G. S. Soh and S. Foong, 2019, "Dynamics and Control of a Collaborative and Separating Descent of Samara Autorotating Wings," in *IEEE Robotics and Automation Letters*, vol. 4, no. 3, pp. 3067-3074, doi: 10.1109/LRA.2019.2924837.

Lee, Sujin & Lee, Eui & Sohn, Myong. (2014). Mechanism of autorotation flight of maple samaras (Acer palmatum). Experiments in Fluids. 55. 10.1007/s00348-014-1718-4.

LEISHMAN, J.G. Principles of Helicopter Aerodynamics, Cambridge University Press, 2002, New York, NY, US.

Appendix A

Project Management

Below are presented Gantt charts for both semesters of 2021/22 academic year that have been developed at the beginning of the project. These plans have not been redesigned.

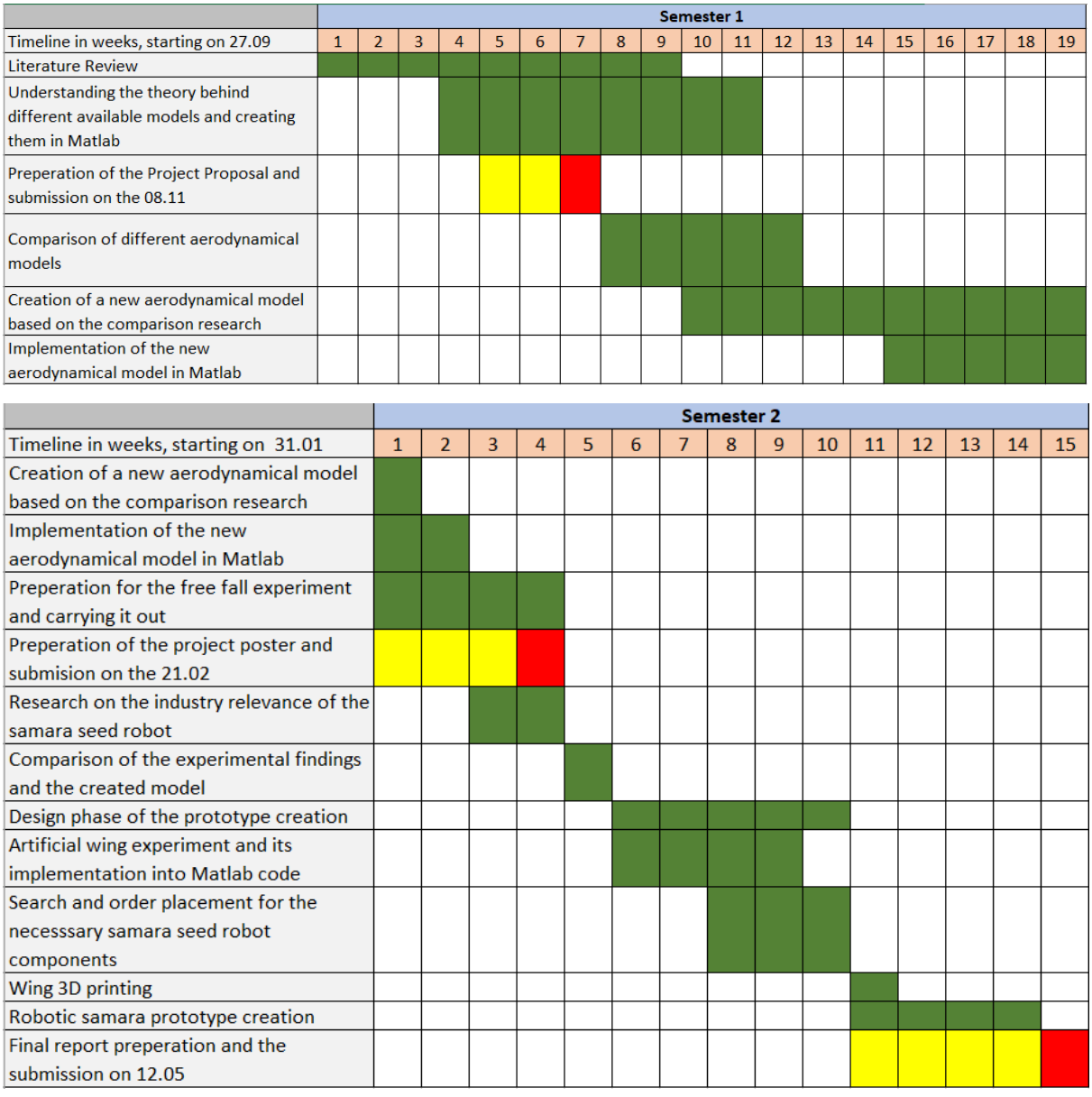

Figure 19 Gantt charts for the project plan (1st draft)

After some reflection on the project management of this individual project, it has been concluded that the first draft of the plan for the project timetable was inconsiderate of work that had to be done for other modules on the course. Sometimes it has been hard to judge how time would one task require as this was the first project of

such scope that has been undertaken. One of the main regrets of the management of the project, has been the insufficient literature review at the beginning of the project which led to indecisiveness in later stages. As the project scope that has been selected at the beginning was very large, this indecisiveness has led to time management problems and delays. Additionally, due to the work that has been required by other modules, there were long periods of time when there was no work done on the project. This led to gaps in knowledge due to simply forgetting where the project was left off last time. However, Easter break was one time in a semester that no other work was required, and it was truly possible to focus on the individual project. Unfortunately, catching Covid-19 during the Easter has not made it easier to work on the project. However, the break from other modules helped immensely and I was able to focus on the individual project. Overall, a great experience has been gained from this project. Further similar projects that could be undertaken in the future will be started with a little more knowledge and a better understanding of good project planning that takes into consideration other factors.

Appendix B

The code developed in this study has been presented below

```
clc
clear
%% Inputs
% CONSTANTS

g = 9.81; % acceleration due to gravity [m/s^2]
rho_air = 1.225; % dnesity of air [kg/m^3]
e = 2.71828; % euler's number constant
mass = 0.00035; % mass of the samra seed [kg]
Cl_alpha_2d = 5.138; % Theorecital 2D aerofoil lift curve
slope
E = 1.125;% Edge correction for Aspect Ratios of 4
k = 1.18;% The k factor to correct the downwash

span = 0.0368; % Span of the wing [m]
chord_root = 0.008; % chord at root of the wing [m]
theta_0 = -7*3.14/180; % datum blade pitch angle relative
to the plane of rotation
theta_t = 0; % local twist but can be simplified to be 0
r = linspace(0.00001,span,80) ; % vector of different
raidal positions [m]

%% shape inputs

% Chord distribution
for i = 1:41
    chord(i) = chord_root+0.24*r(i);
end
for i = 42:52
    chord(i) = chord(41);
end
for i = 53:72
    chord(i) = chord(41)-0.6*r(i-51); % -0.55 & 0.28
end
for i = 73:80
    chord(i) = chord(72)-1.1*r(i-71); % -0.55 & 1.2
end
chord_position = linspace(0,chord(41),30); % Chrodwise
points
chord_distance = chord(41)/29; % distance betweeen points
in chordwise direction
chord_average = sum(chord)/80; % average chord of the
wing [m]
```

```
figure
plot(r,chord)
xlabel('spanwise distance [m]')
ylabel('chord length [m]')

wing_area = span*chord_average; % wing area [m^2]
AR = span^2/wing_area;% Aspect ratio of the wing, usually
is 3-5

% Thickness distribution
% row 1
for y = 1:5
    thick(1,y) = 0.5;
end
for y = 6:17
    thick(1,y) = 0.7;
end
for y = 18:54
    thick(1,y) = 0.5;
end
% row 2
for y = 1:2
    thick(2,y) = 0.5;
end
for y = 3:15
    thick(2,y) = 0.7;
end
for y = 16:58
    thick(2,y) = 0.5;
end
%row 3
for y = 1:13
    thick(3,y) = 0.7;
end
for y = 14:16
    thick(3,y) = 0.5;
end
for y = 17:24
    thick(3,y) = 0.7;
end
for y = 25:45
    thick(3,y) = 0.5;
end
for y = 46:62
    thick(3,y) = 0.25;
end
```

```
% row 4
thick(4,1) = 1;
for y = 2:18
    thick(4,y) = 0.7;
end
for y = 19:39
    thick(4,y) = 0.5;
end
for y = 40:66
    thick(4,y) = 0.25;
end
% row 5
for y = 1:3
    thick(5,y) = 1;
end
for y = 4:14
    thick(5,y) = 0.7;
end
for y = 15:24
    thick(5,y) = 0.5;
end
for y = 25:69
    thick(5,y) = 0.25;
end
% Row 6
for y = 1:3
    thick(6,y) = 1;
end
for y = 4:7
    thick(6,y) = 0.7;
end
for y = 8:19
    thick(6,y) = 0.5;
end
for y = 20:42
    thick(6,y) = 0.25;
end
for y = 43:45
    thick(6,y) = 0.1;
end
for y = 46:52
    thick(6,y) = 0.25;
end
for y = 53:54
    thick(6,y) = 0.1;
end
for y = 55:61
```

```
    thick(6,y) = 0.25;
end
for y = 62:64
    thick(6,y) = 0.1;
end
for y = 65:73
    thick(6,y) = 0.25;
end
% Row 7
for y = 1:4
    thick(7,y) = 1;
end
for y = 5:7
    thick(7,y) = 0.7;
end
for y = 8:22
    thick(7,y) = 0.5;
end
for y = 23:38
    thick(7,y) = 0.25;
end
for y = 39:40
    thick(7,y) = 0.1;
end
for y = 41:44
    thick(7,y) = 0.25;
end
for y = 45:51
    thick(7,y) = 0.1;
end
thick(7,52) = 0.25;
for y = 53:56
    thick(7,y) = 0.1;
end
for y = 57:64
    thick(7,y) = 0.25;
end
for y = 65:68
    thick(7,y) = 0.1;
end
for y = 69:74
    thick(7,y) = 0.25;
end
% Row 8
for y = 1:4
    thick(8,y) = 1;
end
```

```
thick(8,5) = 0.7;
for y = 6:15
    thick(8,y) = 0.5;
end
for y = 16:39
    thick(8,y) = 0.25;
end
for y = 40:43
    thick(8,y) = 0.1;
end
for y = 44:47
    thick(8,y) = 0.25;
end
for y = 48:70
    thick(8,y) = 0.1;
end
for y = 71:75
    thick(8,y) = 0.25;
end
% Row 9
for y = 1:3
    thick(9,y) = 1;
end
thick(9,4) = 0.7;
for y = 5:13
    thick(9,y) = 0.5;
end
for y = 14:30
    thick(9,y) = 0.25;
end
for y = 31:34
    thick(9,y) = 0.1;
end
for y = 35:41
    thick(9,y) = 0.25;
end
for y = 42:45
    thick(9,y) = 0.1;
end
for y = 46:47
    thick(9,y) = 0.25;
end
for y = 48:70
    thick(9,y) = 0.1;
end
for y = 71:76
    thick(9,y) = 0.25;
```

```
end
% Row 10
for y = 1:3
    thick(10,y) = 1;
end
thick(10,4) = 0.7;
for y = 5:7
    thick(10,y) = 0.5;
end
for y = 8:22
    thick(10,y) = 0.25;
end
for y = 23:27
    thick(10,y) = 0.1;
end
for y = 28:32
    thick(10,y) = 0.25;
end
for y = 33:38
    thick(10,y) = 0.1;
end
for y = 39:42
    thick(10,y) = 0.25;
end
for y = 43:46
    thick(10,y) = 0.1;
end
thick(10,47) = 0.25;
for y = 48:72
    thick(10,y) = 0.1;
end
for y = 73:77
    thick(10,y) = 0.25;
end
% Row 11
for y = 1:3
    thick(11,y) = 1;
end
thick(11,4) = 0.7;
for y = 5:6
    thick(11,y) = 0.5;
end
for y = 7:24
    thick(11,y) = 0.25;
end
for y = 25:30
    thick(11,y) = 0.1;
```

```
end
for y = 31:33
    thick(11,y) = 0.25;
end
for y = 34:41
    thick(11,y) = 0.1;
end
for y = 42:44
    thick(11,y) = 0.25;
end
for y = 45:74
    thick(11,y) = 0.1;
end
for y = 75:78
    thick(11,y) = 0.25;
end
% Row 12
for y = 1:3
    thick(12,y) = 1;
end
for y = 4:5
    thick(12,y) = 0.5;
end
for y = 6:18
    thick(12,y) = 0.25;
end
for y = 19:20
    thick(12,y) = 0.1;
end
for y = 21:26
    thick(12,y) = 0.25;
end
for y = 27:34
    thick(12,y) = 0.1;
end
thick(12,35) = 0.25;
for y = 36:44
    thick(12,y) = 0.1;
end
thick(12,45) = 0.25;
for y = 46:75
    thick(12,y) = 0.1;
end
for y = 76:79
    thick(12,y) = 0.25;
end
% Row 13
```

```
for y = 1:2
    thick(13,y) = 1;
end
for y = 3:4
    thick(13,y) = 0.5;
end
for y = 5:12
    thick(13,y) = 0.25;
end
thick(13,13) = 0.1;
for y = 14:17
    thick(13,y) = 0.25;
end
for y = 18:76
    thick(13,y) = 0.1;
end
for y = 77:80
    thick(13,y) = 0.25;
end

% Row 14
thick(14,1) = 1;
for y = 2:4
    thick(14,y) = 0.5;
end
for y = 5:13
    thick(14,y) = 0.25;
end
for y = 14:78
    thick(14,y) = 0.1;
end
for y = 79:80
    thick(14,y) = 0.25;
end
% Row 15
for y = 1:3
    thick(15,y) = 0.5;
end
for y = 4:9
    thick(15,y) = 0.25;
end
for y = 10:80
    thick(15,y) = 0.1;
end
% Row 16
for y = 1:2
    thick(16,y) = 0.5;
```

```
end
for y = 3:10
    thick(16,y) = 0.25;
end
for y = 11:80
    thick(16,y) = 0.1;
end
% Row 17
thick(17,1) = 0.5;
for y = 2:4
    thick(17,y) = 0.25;
end
for y = 5:6
    thick(17,y) = 0.1;
end
for y = 7:11
    thick(17,y) = 0.25;
end
for y = 12:80
    thick(17,y) = 0.1;
end
% Row 18
for y = 1:4
    thick(18,y) = 0.25;
end
for y = 5:79
    thick(18,y) = 0.1;
end
% Row 19
thick(19,1) = 0.25;
for y = 2:77
    thick(19,y) = 0.1;
end
% Row 20
for y = 1:75
    thick(20,y) = 0.1;
end
% Row 21
for y = 1:73
    thick(21,y) = 0.1;
end
% Row 22
for y = 1:71
    thick(22,y) = 0.1;
end
% Row 23
for y = 3:68
```

```
    thick(23,y) = 0.1;
end
% Row 24
for y = 9:66
    thick(24,y) = 0.1;
end
% Row 25
for y = 14:64
    thick(25,y) = 0.1;
end
% Row 26
for y = 19:61
    thick(26,y) = 0.1;
end
% Row 27
for y = 25:59
    thick(27,y) = 0.1;
end
% Row 28
for y = 30:57
    thick(28,y) = 0.1;
end
% Row 29
for y = 35:54
    thick(29,y) = 0.1;
end
% Row 30
for y = 41:52
thick(30,y) = 0.1;
end

thickness = thick*(0.1*chord_average);

thick(thick==0)=nan; % For the purposes of the graph re-
moves 0s
thickness_nan = thick*(0.1*chord_average);
figure
surf(r,chord_position,thickness_nan)
xlabel('spanwise distance [m]')
ylabel('chordwise distance [m]')
grid on
daspect([1 1 1])
view(3)


%% Unknown Inputs
```

```
syms omega V_d v_i beta

%% Aerodynamics
% A MODIFIED NORMAL FORCE MODEL FROM NABAWY'S PAPER HAS
BEEN IMPLEMENTED
Cl_alpha_3D = Cl_alpha_2d/(E+(k*Cl_al-
pha_2d)/(3.14*AR)); % Wing lift curve slope with correc-
tion for 3D effecs

%% Kinematics

V_inplane = omega*r; % velocity of incoming air in plane
of rotation [m/s]
beta_flapping = beta/50; % blade flapping rate
V_upflow = (V_d-v_i)*cos(beta)-beta_flapping.*r; % veloc-
ity of vertical flow
V = sqrt(V_upflow.^2+V_inplane.^2); % combined incoming
airflow velocity [m/s]

phi = atan(V_upflow./V_inplane); % local pitch angle
[rad]
theta = theta_0+theta_t; % blade pitch angle [rad]
alpha = theta+phi; % local angle of attack [rad]

f = 0.5*((1-r/span)./((r/span).*phi)); % some dumb f for
tip loss
eta_tip = (2/3.14)*(acos(e.^(-f))); % tip loss coefficent

%% aerodynamics
Cl = Cl_alpha_3D*sin(alpha).*cos(alpha);
Cd = Cl.*tan(alpha);

L_d = 0.5*rho_air.*V.*chord.*r.*Cl.*eta_tip;
D_d = 0.5*rho_air.*V.*chord.*r.*Cd;

%% Joining both together

T_d = L_d.*cos(phi)+D_d.*sin(phi);
Q_d = (L_d.*sin(phi)-D_d.*cos(phi)).*r;

T_iteration = T_d.*cos(beta);

T = sum(T_iteration);
Q = sum(Q_d);

%% Centrifugal force
% mass distribution
thickness_r = sum(thickness);
```

```
mass_proportions_r = thickness_r/sum(thickness_r);
mass_r = (mass/2)*mass_proportions_r;

F_centrifugal_r = mass_r.*omega^2.*r;
F_centrifugal = sum(F_centrifugal_r);
F_centrifugal_seed = 0.15822*span*(mass/2)*omega^2;

%% Solving for the unknowns

A = 3.14*span^2; % Rotor disc area
T_m = 2*rho_air*A*(V_d-v_i)*v_i; % Thrust predicted from
the momentum analysis

F(1) = T-T_m == 0;
F(2) = T-mass*g == 0;
F(3) = Q == 0;
F(4) = F_centrifugal-T*sin(beta)-F_centrifugal_seed == 0;

[V_d_true,omega_true,v_i_true,beta_true] = vpasolve([F(1)
F(2) F(3) F(4)],[V_d omega v_i beta],[1 40 0.5 0.1])


%% Calculation of true aerodynamic values


V_inplane = omega_true.*r; % velocity of incoming air in
plane of rotation [m/s]
V_upflow = (V_d_true-v_i_true)*cos(beta_true); % velocity
of vertical flow
V = sqrt(V_upflow.^2+V_inplane.^2); % combined incoming
airflow velocity [m/s]

phi = atan(V_upflow./V_inplane); % local pitch angle
[rad]
theta = theta_0+theta_t; % blade pitch angle [rad]
alpha = theta+phi; % local angle of attack [rad]

f = 0.5*((1-r/span)./((r/span).*phi)); % some dumb f for
tip loss
eta_tip = (2/3.14)*(acos(e.^(-f))); % tip loss coefficent

Cl = Cl_alpha_3D*sin(alpha).*cos(alpha);
Cd = Cl.*tan(alpha);

L_d = 0.5*rho_air.*V.*chord.*r.*Cl.*eta_tip;
D_d = 0.5*rho_air*V.*chord.*r.*Cd;

T_d = L_d.*cos(phi)+D_d.*sin(phi);
```

```
Q_d = (L_d.*sin(phi)-D_d.*cos(phi)).*r;
T_iteration = T_d.*cos(beta_true);

figure
plot(r,T_d)
xlabel('Radial distance [m]')
ylabel('Thrust acting on a blade element [N]')

figure
plot(r,Q_d)
xlabel('Radial distance [m]')
ylabel('Torque acting on a blade element [N]')

T = sum(T_iteration);
Q = sum(Q_d);

figure
plot(r,T_d)
%% Flexibility inclusion
% Second moment of area calculations for a cross section
at different
% radial positions

I_x = zeros(1,80);
for i = 1:80
    for j = 1:29
        rectangular(j,i) = (chord_distance*thick-
ness(j,i)^3)/3;
        triangle(j,i) = (chord_distance*(thick-
ness(j+1,i)-thickness(j,i))^3)/6+0.5*chord_dis-
tance*(thickness(j+1,i)-thickness(j,i))*thickness(j,i)^2;
        I_x_point(j,i) = rectangular(j,i)+triangle(j,i);
        I_x(i) = I_x(i)+I_x_point(j,i);
    end
end

% % First wing area - Leading edge
% % It can be simplified to be a beam of certain varying
thickness

E_modulus_range = linspace(0.1*10^9,5*10^9,50);
for iter = 1:50;
E_modulus = E_modulus_range(iter);
% E_modulus = 0.9*10^9;
% iter = 1;

deflection = zeros(1,80);
for i = 1:80
```

```
    for y = 1:80
        if y<=i
            deflection(y) = deflection(y)+(((T_d(i)-
mass_r(i)*g)*r(y)^2)/(6*E_modulus*I_x(y)))*(3*r(i)-r(y));

        elseif y>i
            deflection(y) = deflection(y)+(((T_d(i)-
mass_r(i)*g)*r(i)^2)/(6*E_modulus*I_x(y)))*(3*r(y)-r(i));
        end
    end
end

% p = polyfit(r,deflection,3);
% y1 = polyval(p,r);
% figure
% hold on
% plot(r,y1)
% plot(r,deflection,'o')
% xlabel('radius [m]')
% ylabel('deflection [m]')
% daspect([1 1 1])


beta_deflection = atan(deflection./r);
beta_all = beta_true+beta_deflection;
span_new = sqrt(span^2-(deflection(80))^2);

[V_d_deflection(iter),omega_deflection(iter),v_i_deflec-
tion(iter)] = samara_performance(beta_all)
end

figure
plot(E_modulus_range,V_d_deflection)
xlabel("Young's Modulus [Pa]")
ylabel("Descent Velocity [m/s]")
```

Function used in the above code

```
function [x,y,z,j] = samara_performance(beta)
%% Inputs
% CONSTANTS

g = 9.81; % acceleration due to gravity [m/s^2]
rho_air = 1.225; % dnesity of air [kg/m^3]
e = 2.71828; % euler's number constant
```

```
mass = 0.00035; % mass of the samra seed [kg]

% Theorecital 2D aerofoil lift curve That has been re-
duced to mach samara
% seeds at low Reynolds number (Nabawy's part 2)
Cl_alpha_2d = 5.138;
% Edge correction for Aspect Ratios of 4 based on Jones:
https://www.resear
% chgate.net/figure/The-edge-correction-Variation-of-the-
Jones-edge-correct
% ion-E-for-different_fig4_280910437
E = 1.125;
% The k factor to correct the downwash, estimated for now
due to not much
% time part 1 and part 2 Mostafa's papaers
k = 1.35;

% KINEMATICS INPUTS

% syms omega V_d v_i

syms V_d omega v_i


% WING SHAPE INPUTS

span = 0.0368; % Span of the wing [m]
chord_root = 0.008; % chord at root of the wing [m]


r = linspace(0.00001,span,80) ; % vector of different
raidal positions [m]

% Chord distribution
for i = 1:41
    chord(i) = chord_root+0.24*r(i);
end
for i = 42:52
    chord(i) = chord(41);
end
for i = 53:72
    chord(i) = chord(41)-0.6*r(i-51); % -0.55 & 0.28
end
for i = 73:80
    chord(i) = chord(72)-1.1*r(i-71); % -0.55 & 1.2
end
chord_position = linspace(0,chord(41),30);
```

```
chord_distance = chord(41)/29; % distance betweeen points
in chordwise direction

% average chord of the wing [m]
chord_average = sum(chord)/80;


beta_flapping = beta./50; % blade flapping rate jsut for
now
theta_0 = -7*3.14/180; % datum blade pitch angle relative
to the plane of rotation
theta_t = 0; % local twist but can be simplified to be 0

%% Samara seed shape
% average chord of the wing [m]
chord_average = sum(chord)/80;

% wing area [m^2]
wing_area = span*chord_average;

% Aspect ratio of the wing, usually is 3-5
AR = span^2/wing_area;

%% Aerodynamics
% A MODIFIED NORMAL FORCE MODEL FROM NABAWY'S PAPER HAS
BEEN IMPLEMENTED

% Wing lift curve slope with correction for 3D effecs
from Prandtl's theory
% described in Nabawy's part 2
Cl_alpha_3D = Cl_alpha_2d/(E+(k*Cl_alpha_2d)/(3.14*AR));

% Mostafa Nabawy's modified normal force model (The role
of the leading
% edge vortex in lift augmentation of steadily revolving
wings: a change
% in perspective)
% Cl = Cl_alpha_3D*sin(alpha)*cos(alpha);
% Cd = Cl*tan(alpha);

%% Kinematics
% All the neccessary variables will be calculated at dif-
ferent radial
% distances from the centre of rotation to account for
different flow
% conditions and shape differences
```

```
V_inplane = omega.*r; % velocity of incoming air in plane
of rotation [m/s]
V_upflow = (V_d-v_i)*cos(beta)-beta_flapping.*r; % veloc-
ity of vertical flow
V = sqrt(V_upflow.^2+V_inplane.^2); % combined incoming
airflow velocity [m/s]

phi = atan(V_upflow./V_inplane); % local pitch angle
[rad]
theta = theta_0+theta_t; % blade pitch angle [rad]
alpha = theta+phi; % local angle of attack [rad]

f = 0.5*((1-r/span)./((r/span).*phi)); % some dumb f for
tip loss
eta_tip = (2/3.14)*(acos(e.^(-f))); % tip loss coefficent


%% aerodynamics
Cl = Cl_alpha_3D*sin(alpha).*cos(alpha);
Cd = Cl.*tan(alpha);

L_d = 0.5*rho_air.*V.*chord.*r.*Cl.*eta_tip;
D_d = 0.5*rho_air*V.*chord.*r.*Cd;

%% Joining both together

T_d = L_d.*cos(phi)+D_d.*sin(phi);
Q_d = (L_d.*sin(phi)-D_d.*cos(phi)).*r;

T_iteration = T_d.*cos(beta);

T = sum(T_iteration);
Q = sum(Q_d);

%% Solving for the unknowns

A = 3.14*span^2; % Rotor disc area
T_m = 2*rho_air*A*(V_d-v_i)*v_i; % Thrust predicted from
the momentum analysis

F(1) = T-T_m == 0;
F(2) = T-mass*g == 0;
F(3) = Q == 0;

[x,y,z] = vpasolve([F(1) F(2) F(3)],[V_d omega v_i],[1 40
0.5]);
end
```